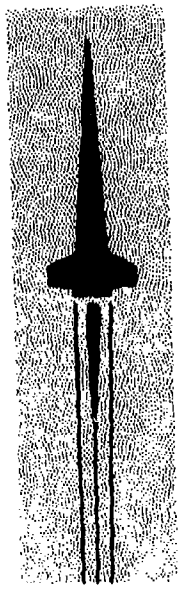

U.S. ARMY MISSILE RESEARCH AND DEVELOPMENT COMMAND

Redstone Arsenal, Alabama 35809

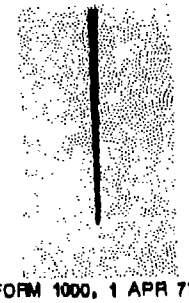

DMI FORM 1000, 1 APR 77

(12)

TECHNICAL REPORT ET-77-8

CALIBRATION AND USE OF B DOT PROBES FOR ELECTROMAGNETIC Measurements

Test and Evaluation Directorate
Engineering Laboratory

9 August 1977

DISPOSITION INSTRUCTIONS

DESTROY THIS REPORT WHEN IT IS NO LONGER NEEDED. DO NOT RETURN IT TO THE ORIGINATOR.

DISCLAIMER

THE FINDINGS IN THIS REPORT ARE NOT TO BE CONSTRUED AS AN OFFICIAL DEPARTMENT OF THE ARMY POSITION UNLESS SO DESIGNATED BY OTHER AUTHORIZED DOCUMENTS.

TRADE NAMES

USE OF TRADE NAMES OR MANUFACTURERS IN THIS REPORT DOES NOT CONSTITUTE AN OFFICIAL INDORSEMENT OR APPROVAL OF THE USE OF SUCH COMMERCIAL HARDWARE OR SOFTWARE.

UNCLASSIFIED

SECURITY CLASSIFICATION OF THIS PAGE (When Data Entered)

REPORT DOCUMENTATION PAGE	READ INSTRUCTIONS BEFORE COMPLETING FORM
1. REPORT NUMBER: ET-77-8 ✓	2. GOVT ACCESSION NO.
3. RECIPIENT'S CATALOG NUMBER	
4. TITLE (and Subtitle): CALIBRATION AND USE OF B DOT PROBES FOR ELECTROMAGNETIC MEASURING	5. TYPE OF REPORT & PERIOD COVERED: Technical Report
6. PERFORMING ORG. REPORT NUMBER: ET-77-8	
7. AUTHOR(s): George R. Edlin, Wayne T. Hudson, and Thomas H. Shumpert	8. CONTRACT OR GRANT NUMBER(s)
9. PERFORMING ORGANIZATION NAME AND ADDRESS: Commander, US Army Missile Research and Development Command, Attn: DRDMI-ET, Redstone Arsenal, Alabama 35809 ✓	10. PROGRAM ELEMENT, PROJECT, TASK AREA & WORK UNIT NUMBERS: AMCMS 738017.B0Q10191
11. CONTROLLING OFFICE NAME AND ADDRESS: Commander, US Army Missile Research and Development Command, Attn: DRDMI-TI, Redstone Arsenal, Alabama 35809	12. REPORT DATE: 9 Aug 77; 13. NUMBER OF PAGES: 60
14. MONITORING AGENCY NAME & ADDRESS (if different from Controlling Office)	15. SECURITY CLASS. (of this report): Unclassified
	15a. DECLASSIFICATION/DOWNGRADING SCHEDULE

16. DISTRIBUTION STATEMENT (of this Report)

Approved for public release; distribution unlimited.

DDC AVAILABILITY NOTICE JAN 20 1978 RESTRICTED F

17. DISTRIBUTION STATEMENT (of the abstract entered in Block 20, if different from Report)

18. SUPPLEMENTARY NOTES

19. KEY WORDS (Continue on reverse side if necessary and identify by block number)

Single-gap probe
Double-gap probe
Electromagnetic field leveling

20. ABSTRACT (Continue on reverse side if necessary and identify by block number)

Modern electromagnetic radiation testing techniques require accurately calibrated field probes that can operate over a wide range of frequencies, without adjustments. This requirement is an outgrowth of the use of wideband radio frequency amplifiers and computer-controlled swept frequency generators. The computer can control the field strength accurately only if accurate sensor information is continuously available. One type of sensor that fulfills this

ABSTRACT (Continued)

DD FORM 1 JAN 73 1473 EDITION OF 1 NOV 65 IS OBSOLETE

UNCLASSIFIED

SECURITY CLASSIFICATION OF THIS PAGE (When Data Entered)

410 164

ABSTRACT (Concluded)

requirement is the B dot probe. The B dot probe is a matched 50-ohm multigap loop which measures dB/dt according to Faraday's law. To assure the accuracy of the probes, a calibration against the National Bureau of Standards' standard dipoles is required. From this calibration data a polynomial is developed which when multiplied times the output of the probe in milliwatts will give the actual field strengths. The output of a digital power meter is fed into the computer which applies the calibration polynomial and allows a real-time electromagnetic field leveling to be accomplished. This technique is applicable any time a broadband electromagnetic leveled field is required.

This study also outlines the design and construction of a single-ended 50-ohm B dot probe, as well as the calibration and development of the required calibration polynomial for computer use.

CONTENTS

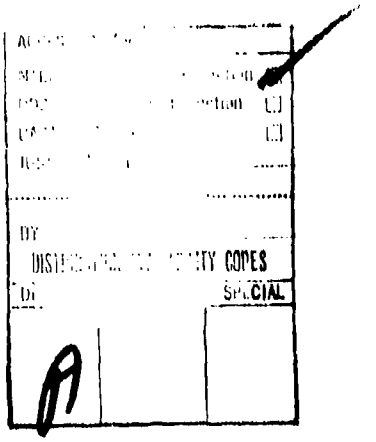

I. INTRODUCTION

A. Background

Conventional field measuring is divided into three categories. The technique used is based on the frequency band that is to be measured. The low frequency band (below 30 MHz) uses standard loop techniques. The medium frequencies (30 MHz to 1 GHz) utilizes standard dipoles. Standard gain horns are used for the frequencies exceeding 1 GHz. This study addresses the frequency range referred to previously as medium frequency (30 MHz to 1 GHz).

The use of computers to completely control the electromagnetic environment, i.e., frequency, modulation, and field strength, makes it highly desirable to have a probe which will measure field strength accurately and not require mechanical adjustments. This requirement makes use of standard dipoles unsatisfactory because the dipoles need to be tuned to their resonant frequency to make the required measurement. The B dot probe, however, has an output that is proportional to the probe area, frequency, and field strength as follows:

$$V_p = \frac{2\pi \ Aeq \ f \ E_o}{c} \quad ,$$

where

Aeq = equivalent area

f = frequency (Hz)

E_o = electric field

c = speed of light (3×10^8 m/sec).

This basic equation along with the correction factor for cable loss gives agreement with the National Bureau of Standards' (NBS) standard with maximum error of approximately 30% as shown in Figure 1. The curve on Figure 1 is a seventh order polynomial fit of the data from the B dot probe in a standard field setup by the NBS dipoles. The calibration accuracy of the NBS standard dipoles is better than ±0.5 dB. The use of this technique makes it possible to sweep rapidly through a broadband of frequencies and maintain a leveled E-field equal to ±1 dB.

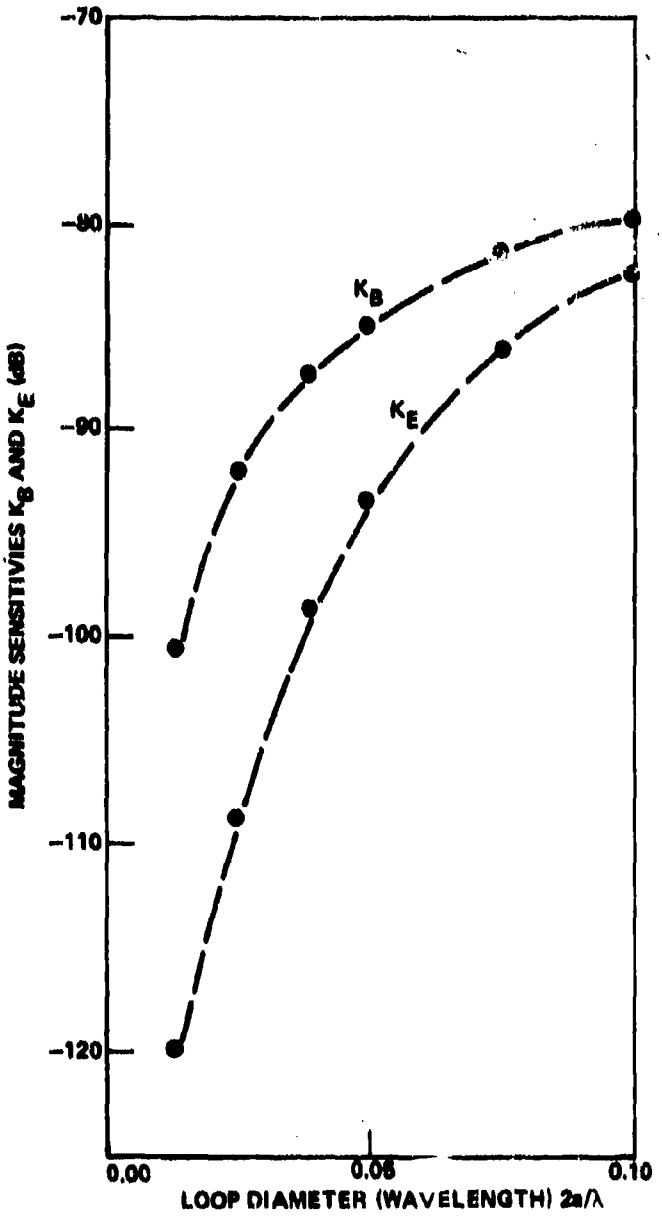

Figure 1. Experimental sensitivities of a single-loaded circular loop [3].

B. Outline of Problem and Solution

The problem which initiated this study was the US Army Missile Command's need for accurate broadband E-field measuring for use in missile system testing. This work outlines the development and calibration of a probe that solves the major problem associated with broadband E-field measuring (i.e., mechanical adjustment requirements). This allows the probe to be interfaced with a computer. The accurate calibration of the probe using NBS standard dipoles solves the remaining problem, which is the required accuracy of the E-field measurement. The 50-ohm double-gap, single-ended loop probe described in this study is an accurately calibrated E-field probe suitable for broadband computerized field measuring and controlling.

II. DESIGN AND CONSTRUCTION OF THE B DOT PROBE

A. Theory of Operation

The basic theory of operation of the B dot loop sensor follows from Faraday's law of induction. The integral of the electric field around the periphery of a loop is equal to the surface integral of the time rage of change of the magnetic induction over the area of the loop; i.e.,

$$-\oint \bar{E} \cdot d\bar{\ell} = \frac{d}{dt} \int \bar{B} \cdot d\bar{s} \quad , \tag{1}$$

where E is the electric field in volts/meter and B is the magnetic flux density in webers/square meter or teslas. Evaluation of the equation around the loop with a sensor radius, a, gives an expression for the total voltage across the loop load gaps:

$$V_{gap} = -[A_{eq}] \frac{dB}{dt} \tag{2}$$

where A_{eq} is the equivalent area of the loop and B is the component of the magnetic flux density along the loop axis. Solving for the incident field component in terms of the probe voltage output,

$$E^{INC} = \frac{c}{A_{eq}} \int V_{gap} \, dt \quad , \tag{3}$$

where c is the speed of light. Thus, the incident electric field may be measured using the output of a properly designed B dot sensor and a time integration of the probe voltage.

B. B Dot Loop Frequency Response

The basic limitation to the frequency response of a B dot loop is the transit time of the current around the loop. This time represents a time dispersion introduced into the signal by the loop dimensions. The loop transit time represents the fastest possible rise time of the B dot sensor and is given by

$$\tau_T = \frac{2\pi a}{c} \quad , \tag{4}$$

where a is loop radius and c is speed of light. From this, one can calculate the maximum frequency response of the loop as

$$f_{max} = \frac{0.35}{\tau_T} = \frac{0.35\ c}{2\pi a} \tag{5}$$

for the 10 to 90% rise time and 3-dB roll-off point.

Another basic limitation of the B dot loop is the low frequency inductance of the loop structure. If a simplified lumped parameter model of the loop is assumed, the sensor rise time may be estimated from the L/R circuit time constant. The 10 to 90% rise time can be approximated as

$$\tau_L = 2.2\ \frac{L}{R} \quad , \tag{6}$$

where R is the total resistance about the loop and L is the loop inductance and is approximately

$$L \simeq \frac{\mu_0\ \pi a^2}{h} \simeq \frac{120\ \pi}{c}\ \frac{\pi a^2}{h} \quad , \tag{7}$$

where h is the length of the cylinder.

By equating the loop transit time [Equation (4)] with the sensor rise time [Equation (6)] and substituting for the loop inductance [Equation (7)], the following dimension constraint emerges:

$$\frac{h}{a} = \frac{2.2\ (60)\ \pi}{R} \quad . \tag{8}$$

If these dimension ratios are attainable, then a loop of this kind can be used to optimize the frequency response by lowering the loop inductance to the point where this limitation is the same as the transit time limitation [1].

C. Loop Analysis

This section presents a summary of the analysis presented by Mory, et al. [2] and Whiteside and King [3]. The following two-dimensional coordinate system is used with the loop oriented in the xy plane and a coordinate, s, along the loop circumference.

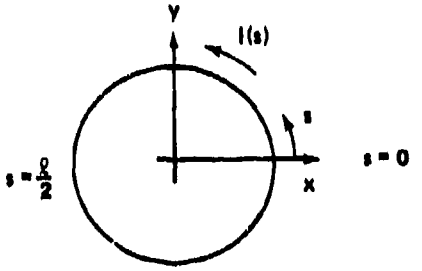

If the loop is used as a field sensor, it sustains not only the usual circulating current proportional to the normal magnetic field but also certain other currents which depend on the average electric field in the plane of the loop rather than on the normal component of the magnetic field. The current may be divided into two components.

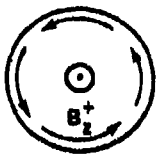

MAGNETIC FIELD CIRCULATING CURRENTS $I^{(0)}$

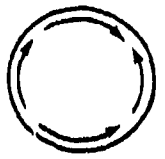

DIPOLE MODE CURRENTS $I^{(1)}$

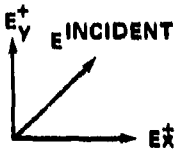

INCIDENT FIELD

The total current at any point, s, and at another point, $s + \ell/2$, can be expressed as

$$I(s) = I^{(0)}(s) + I^{(1)}(s) \tag{9}$$

$$I(s + \ell/2) = I^{(0)}(s) - I^{(1)}(s) \quad , \tag{10}$$

where $I^{(0)}$ is a measure of the magnetic field and $I^{(1)}$ at the top and left subtracts, and at the bottom and right adds.

The dipole mode currents, $I^{(I)}$, may be divided into components resulting from E_x incident and E_y incident.

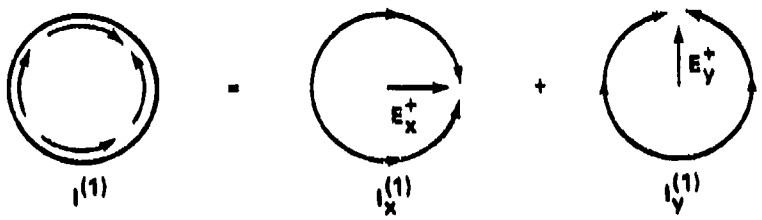

If load points at $s = 0$ and $s = \ell/2$ are considered, $I^{(I)}$ may be neglected because it cancels at these points. Also, at $s = +\ell/4$ and $s = -\ell/4$, $I_y^{(1)} = 0$. The analysis of Whiteside and King [3] presents the values at $s = 0$ as

$$I^{(0)}(0) \simeq \lambda K_B c B_Z^{INC} \tag{11}$$

$$I_y^{(1)}(0) \simeq \lambda K_E E_y^{INC} \tag{12}$$

for the currents for the magnetic field circulating mode and the dipole mode. The constants K_B and K_E are the unloaded magnetic and electric sensitivities dependent upon the loop geometry.

The total load current I_L will be affected by load position and the number of load points. For a singly loaded loop, loaded at $s = 0$,

$$I_L = I(0) = I^{(0)}(0) + I^{(1)}(0) = I^{(0)} + I_x^{(1)}(0) + I_y^{(1)}(0)$$

$$= I^{(0)}(0) + I_y^{(1)}(0) = K_B^{(1)} c B_Z^{INC} + K_E^{(1)} E_y^{INC} \quad . \tag{13}$$

Similarly, if the loop is loaded at $s = \ell/2$,

$$I_L' = I\left(\frac{\ell}{2}\right) = \lambda K_B^{(1)} c B_Z^{INC} - \lambda K_E^{(1)} E_y^{INC} \quad . \tag{14}$$

If the sensor is to be used as a B dot probe, the unwanted electric field terms may be eliminated by using the sum of I_L and I_L' with a doubly-loaded loop and a summing network. Another method of eliminating the electric field term is to use a singly-loaded loop in a known linear polarization field and position the load side of the loop perpendicular to the electric field so that the electric term is eliminated (at $s = 0$ and $s = \pm\ell/2$ for a known polarization, E_x incident).

Experimental sensitivities for singly-loaded and doubly-loaded circular loops may be found in references 2 and 3. Very large errors may be produced by a singly-loaded loop when measuring an unknown polarization field unless the loop diameter, 2a, is small ($2a < 0.01\ \lambda$). For a loop diameter of $2a = 0.1\ \lambda$, the loop responds as strongly to the electric field in the dipole mode as it does to the magnetic field in the circulating mode (Figure 1).

A double-loaded sensor of diameter $2a \leq 0.15\ \lambda$ will function without appreciable interference from the electric field (Figure 2).

D. Pulse Impedance Matching

1. Four-Gap Loop with Balanced, 100-ohm Output

Detailed design information for a four-gap, B dot sensor may be found in reference 2. This sensor utilizes series and parallel combinations of signals from the four gaps to effectively produce a half turn loop. Figures 3 [4] through 6 show the impedance matching technique and the layout of the load gaps around the loop.

Neglecting internal losses and probe reactance, an idealized equivalent circuit of the four-gap probe is shown in the following sketch:

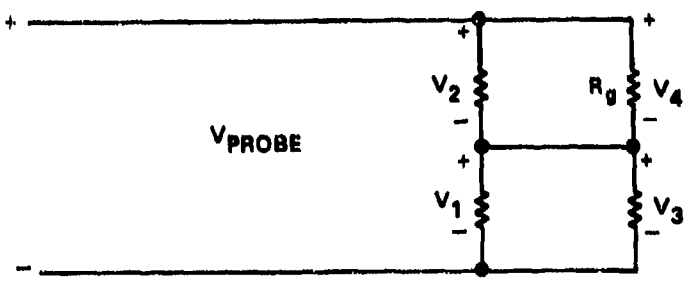

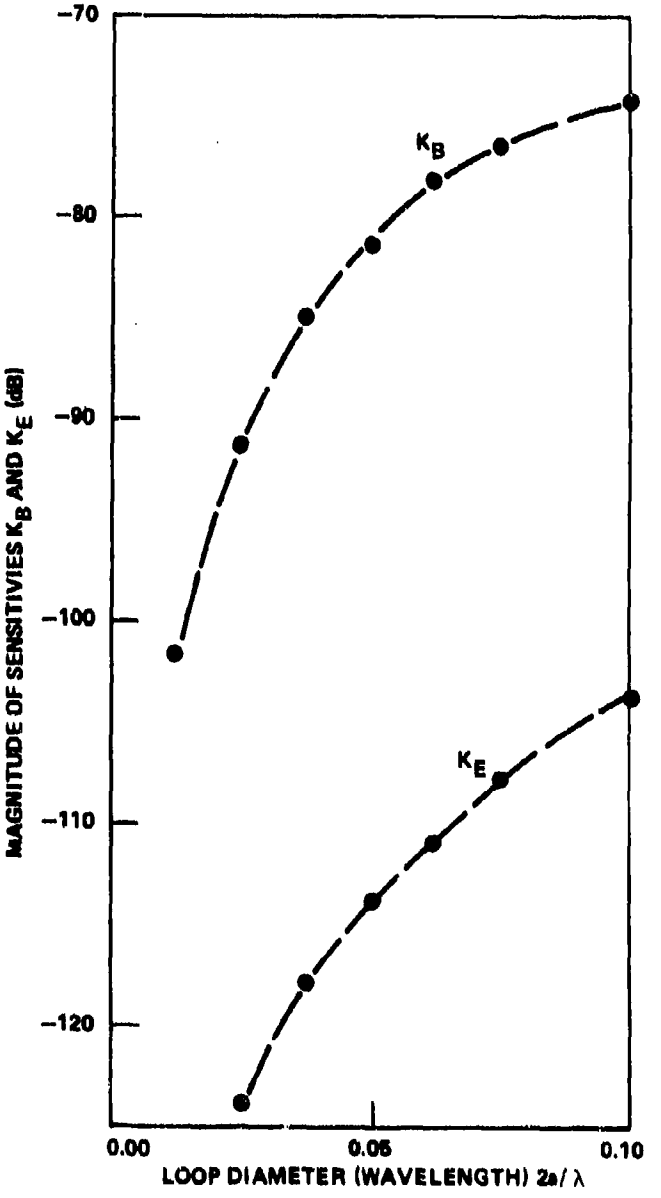

Figure 2. Experimental sensitivities of a double-loaded circular loop [3].

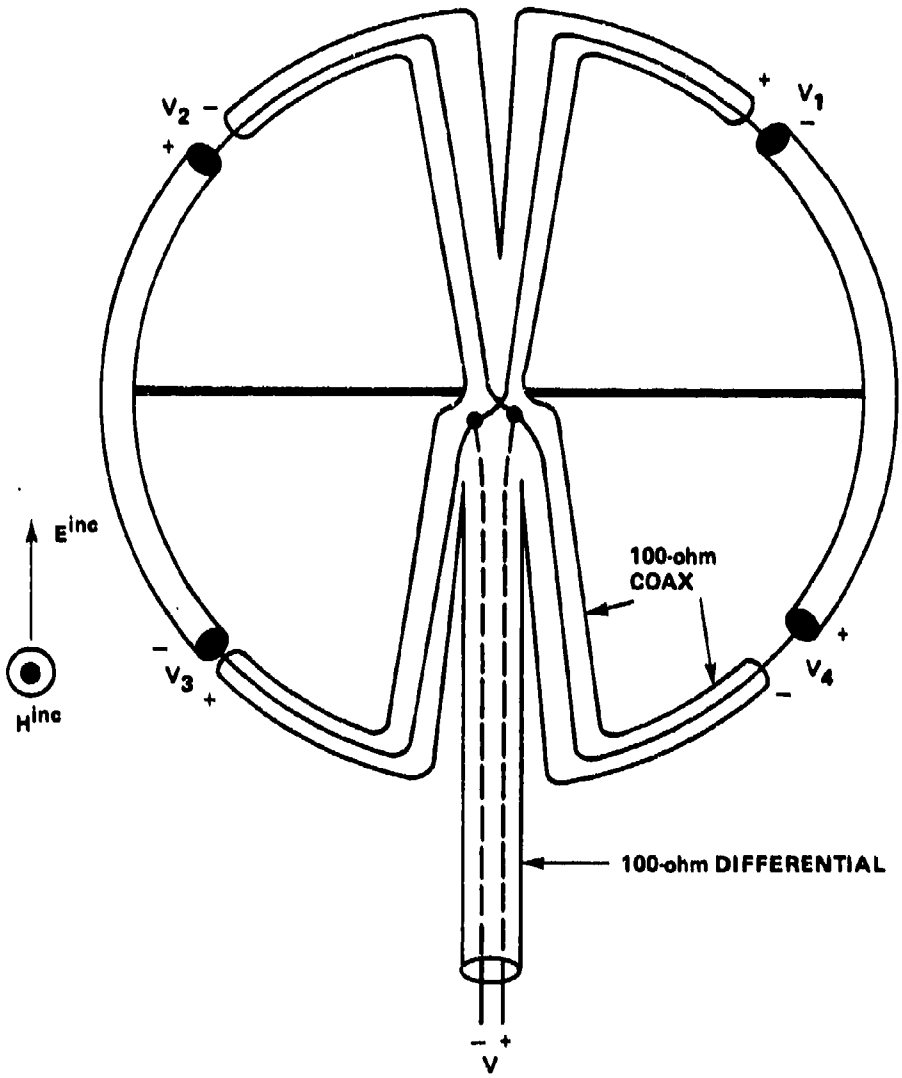

Figure 3. Azimuthal distribution of signal inputs for the four-gap loop [4].

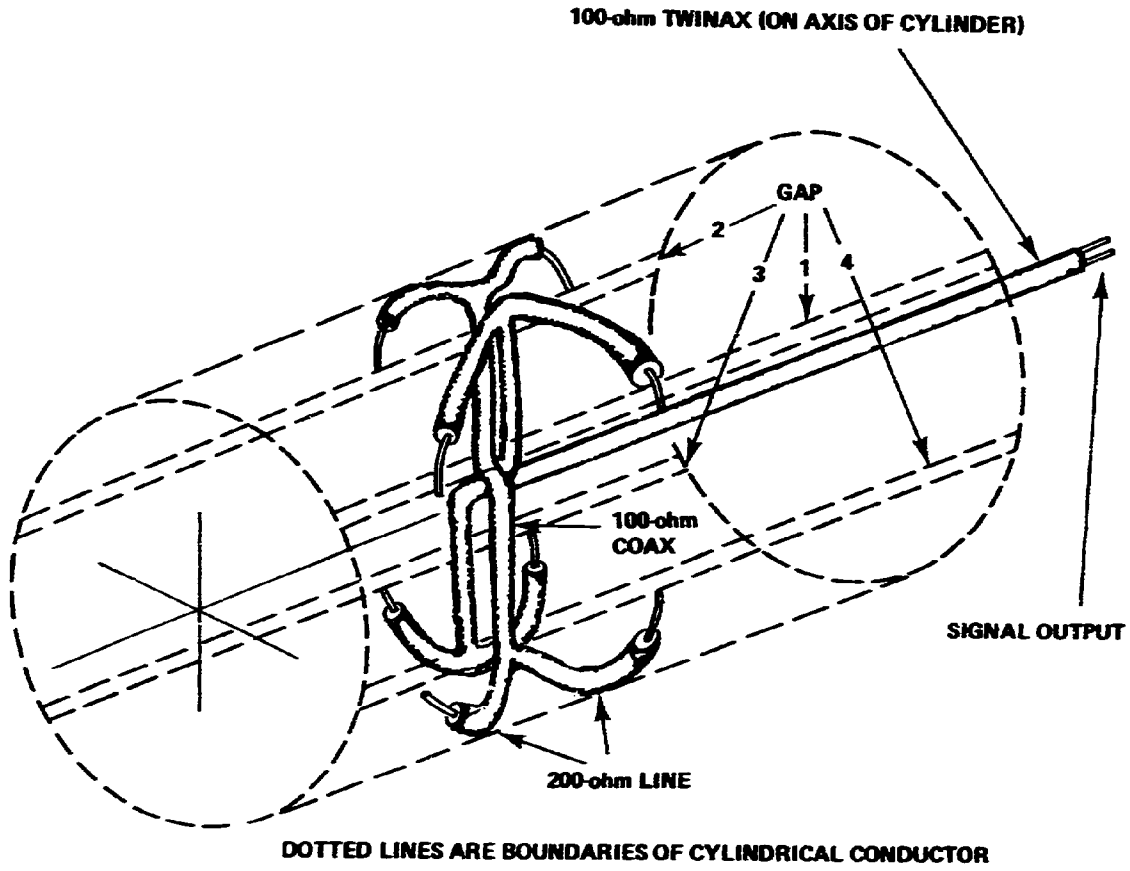

Figure 4. One-half turn cylindrical loop, with axial and azimuthal distribution of signal input [2].

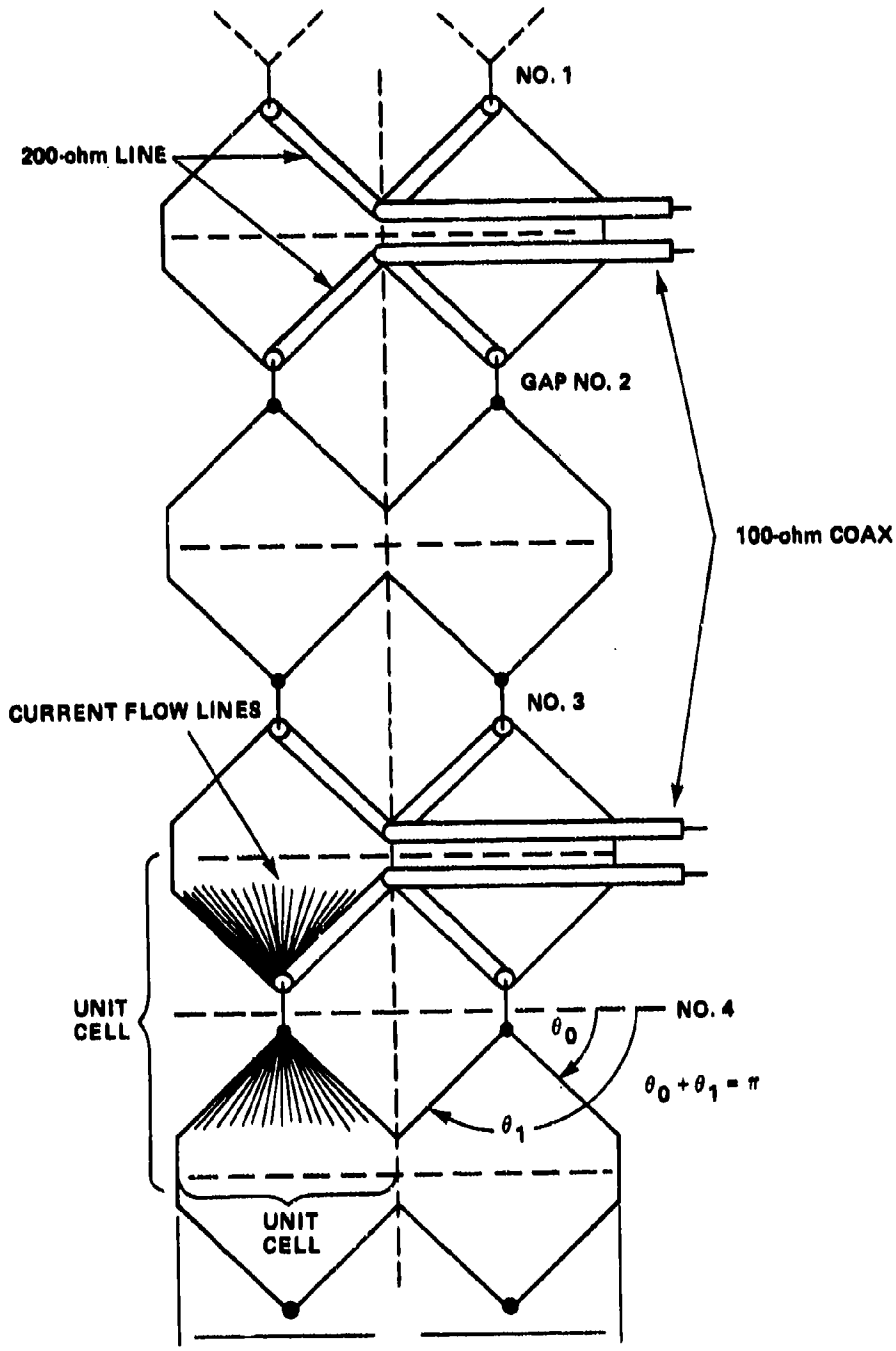

Figure 5. Expanded view of four-gap cylindrical loop using conical transmission line for gaps [2].

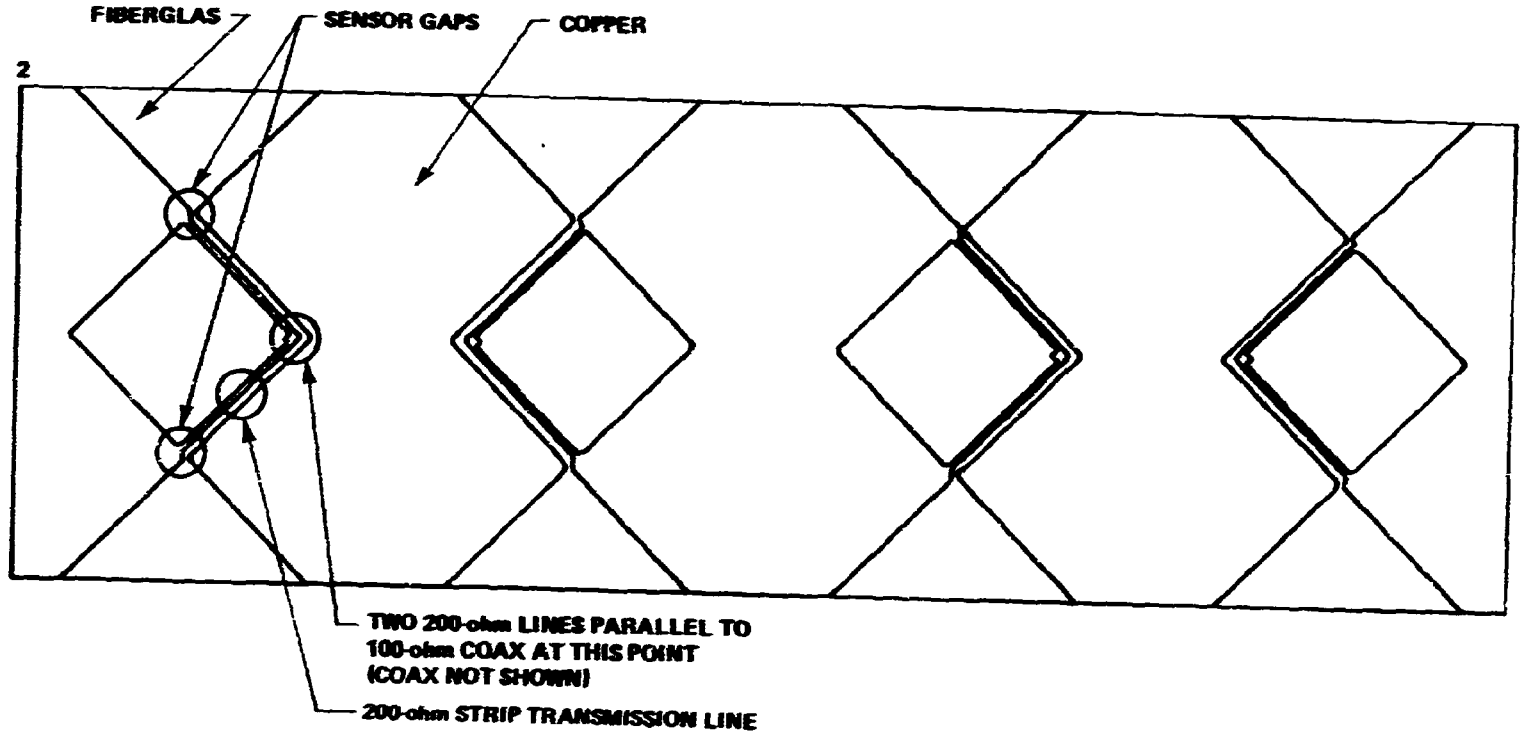

Figure 6. MGL-2A printed circuit board [2].

From this circuit it can be seen that the probe output, $V_p = 1/2\ (V_1 + V_2 + V_3 + V_4)$; this is the equivalent of a half turn loop. The pulse impedance of each gap consists of two parallel conical 200-ohm transmission lines (with $\theta \simeq 49$ deg), resulting in an effective gap pulse impedance, R_g, of 100 ohms in the manner discussed by Baum [5]. Figure 7 shows the pulse impedance variation with an angle for a conical transmission line.

Gap currents directly opposite on the loop are summed to eliminate the electric field current terms in the manner illustrated in Equations (13) and (14). Furthermore, the opposing pairs of gap voltages are effectively series connected to obtain a balanced, double-ended output. The balanced output was utilized to take advantage of common mode signal rejection properties.

2. Double-Gap Loop with Unbalanced 50-ohm Output

If half of the balanced four-gap probe is constructed, a two-gap, unbalanced probe results with an output of 50 ohms:

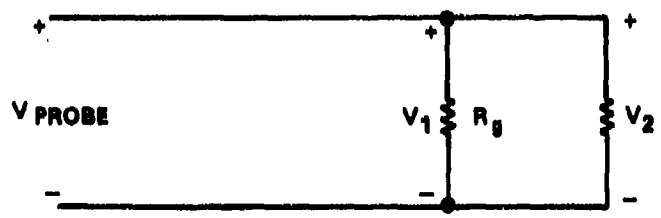

It can be seen that the two gap voltages are paralleled, the V probe = $(V_1 + V_2)/2$, and the loop has effectively a half turn.

Gap voltages directly opposite on a loop diameter are summed to eliminate the electric field current terms [Equations (13) and (14) as in the four-gap loop design previously discussed]. Each gap is fed in two points so that the resistive gap loading is more uniform along the loop axis. The pulse impedance of each gap is adjusted to 200 ohms by use of conical transmission line impedance values derived by Baum [6]. A gap angle of 49 deg was used to obtain two 200-ohm conical transmission lines in parallel.

Each feed point of each gap is connected by a section of 200-ohm microstrip transmission line. Impedance curves for the microstrip line are shown in Figure 8 [7]. The material used for the probe is 1/32-in. polyguide and is copper clad on both sides. The material is a product of Electronized Chemicals Corporation. A 200-ohm characteristic

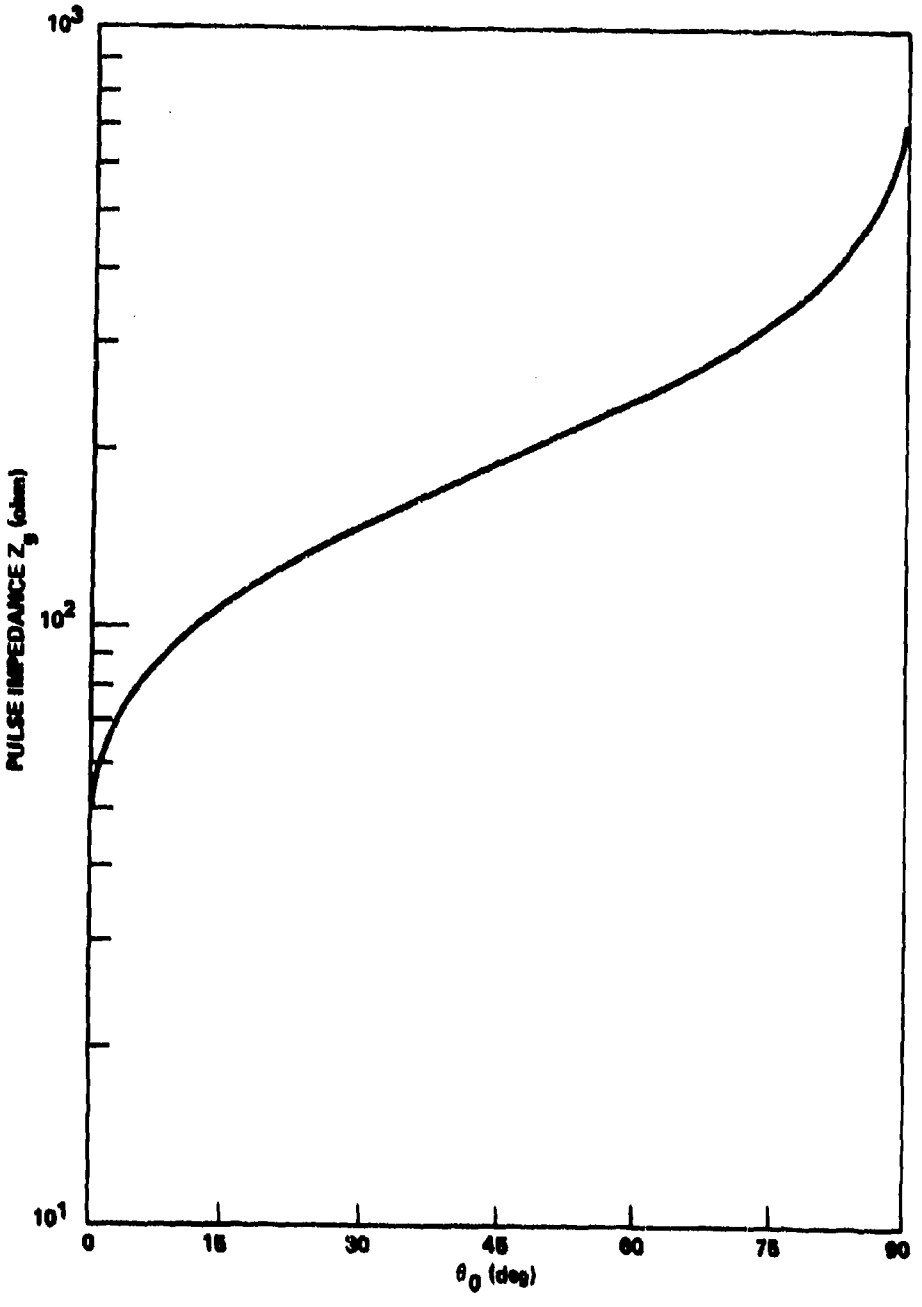

Figure 7. Pulse impedance of conical transmission [5].

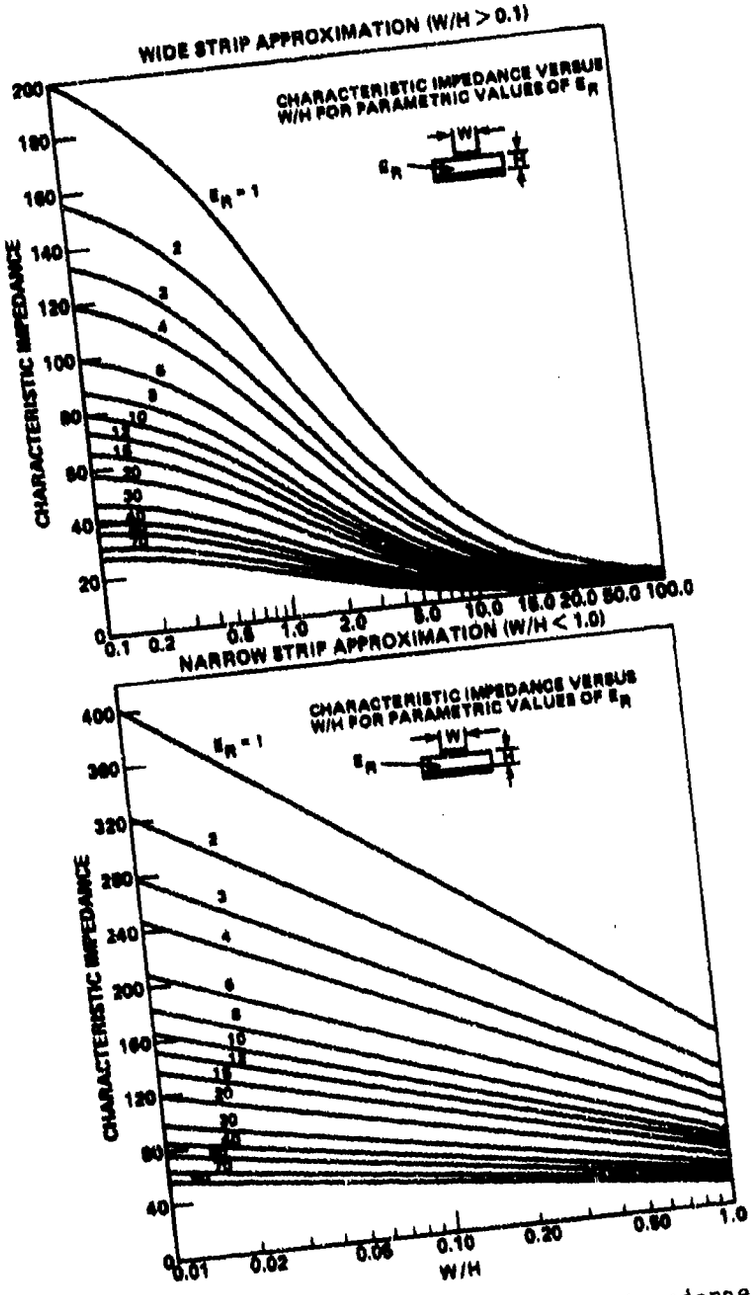

Figure 8. Microstrip characteristic impedance [7].

impedance for $E_R = 2.33$ results in a line width of 0.0031 in. A #43 copper wire cemented to the polyguide surface gave an impedance very close to the desired 200 ohms (Figure 7).

The two 200-ohm microstrip lines junction into a single 100-ohm section of microstrip line. This section is in turn junctioned into a section of 100-ohm semirigid coaxial cable which forms the output of a single gap fed in two points. The 100-ohm semirigid coaxial cable is positioned along a loop diameter, each end of which is fed by each gap. A 50-ohm section of semirigid coaxial cable junctions at the center of the 100-ohm cable and runs along the loop axis.

The removal of the material in the diamond pattern along the probe gap has two beneficial effects on probe operation. First, two 200-ohm conical transmission lines are formed in the gap region, minimizing impedance discontinuities. Secondly, gap capacitance appearing in parallel with the cable impedance is reduced, thereby improving the high frequency response. The inductance of the loop, however, is slightly increased, thereby degrading the high frequency response.

E. Time Domain Reflectometry Measurements

Pulse impedance measurements for the 1.75-in. diameter double-gap probe design were first performed on a single-gap section of the circuit board to check the calculated impedances. The gaps were fed with two 200-ohm sections of twin line [1] junctioning into a section of 93-ohm coaxial cable as shown in Figure 9. The time domain reflectometry (TDR) measurement for this single-gap section is shown in Figure 10. Note that the gap impedance is disturbed by the feed arrangement and part of the signal is on the outside of the coaxial cable.

It was then decided to reconfigure the feed arrangement by using 200-ohm sections of microstrip as gap feeds on the reverse side of the circuit board. These two sections were junctioned into a 100-ohm section of microstrip and then into a section of 93-ohm semirigid coaxial cable. It would have been more desirable to use 100-ohm semirigid cable but none was available in the laboratory. This feeding arrangement has the advantage of getting the gap signal into a coaxial configuration that is normal to the circuit board and that has a 50-ohm output to a cable located along the probe axis. Furthermore, the gap signal is fully contained inside the coaxial cable and not partially on the outside of the cable. The circuit board used for measuring the pulse impedance of a single gap is shown in Figure 11. The measured TDR plot is shown in Figure 12. Note that the gap impedance combination of two parallel 200-ohm conical transmission lines measures nearly 100 ohms, as predicted by Baum [5].

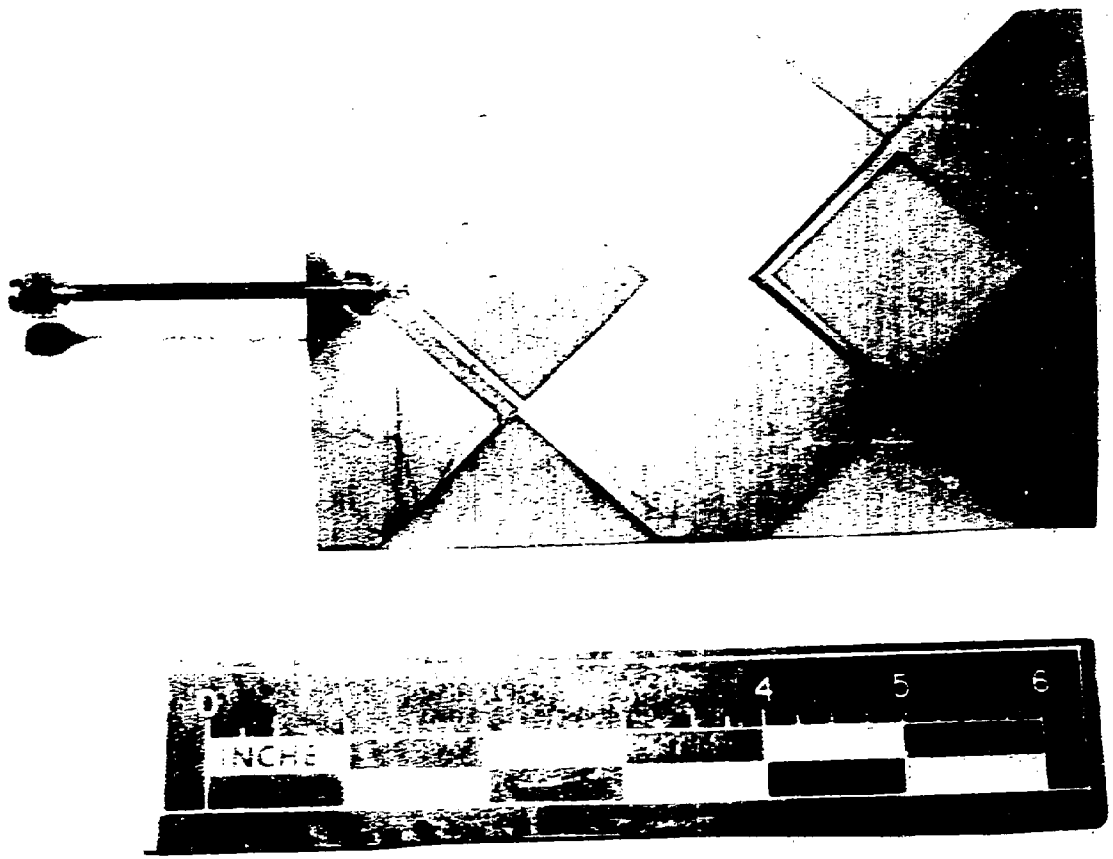

Figure 9. Circuit board for 1.75-in. diameter double-gap probe using twin line gap feeds.

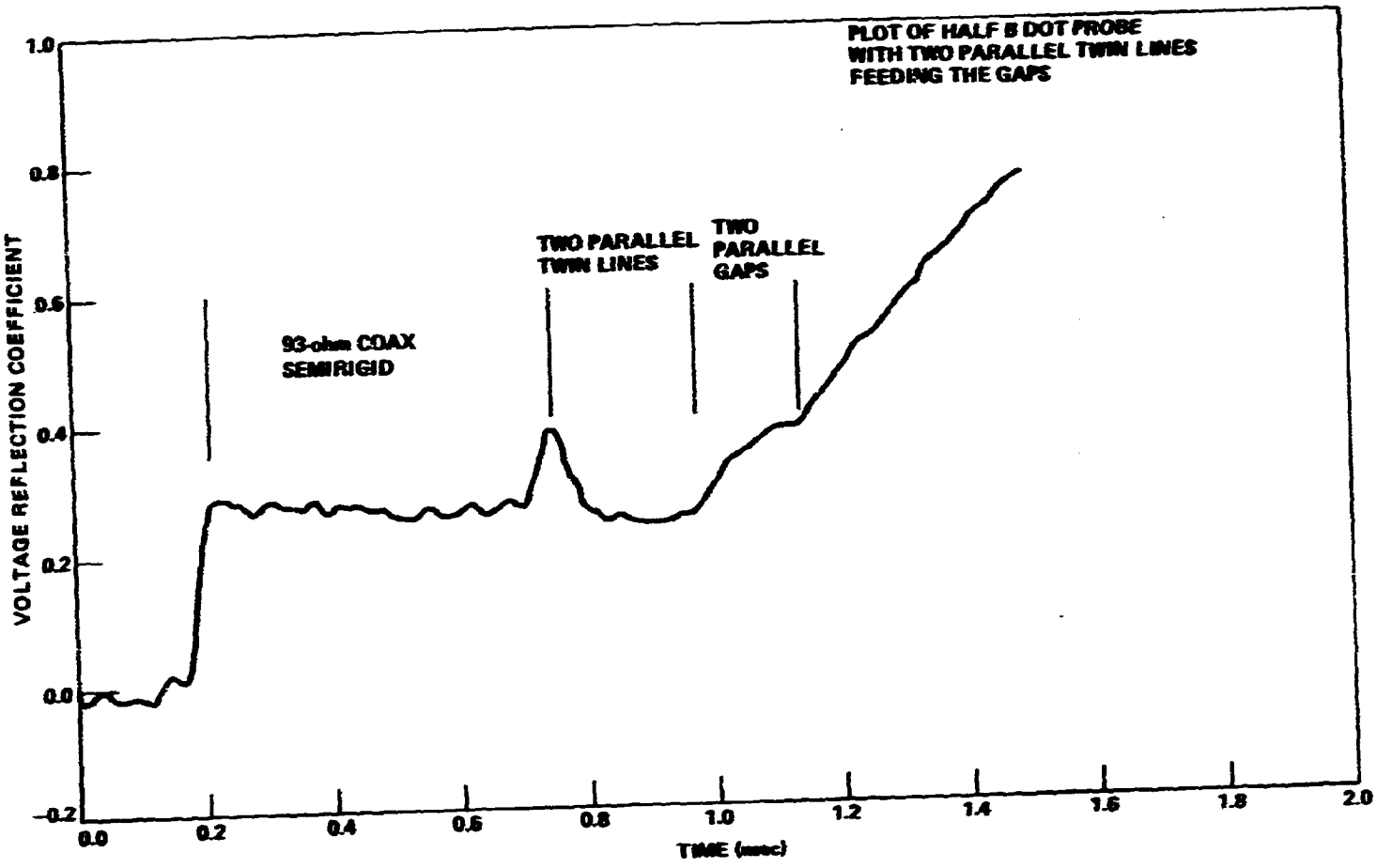

Figure 10. TDR measurement of unassembled 1.75-in. diameter B dot sensor with two parallel twin lines feeding a single gap at two points.

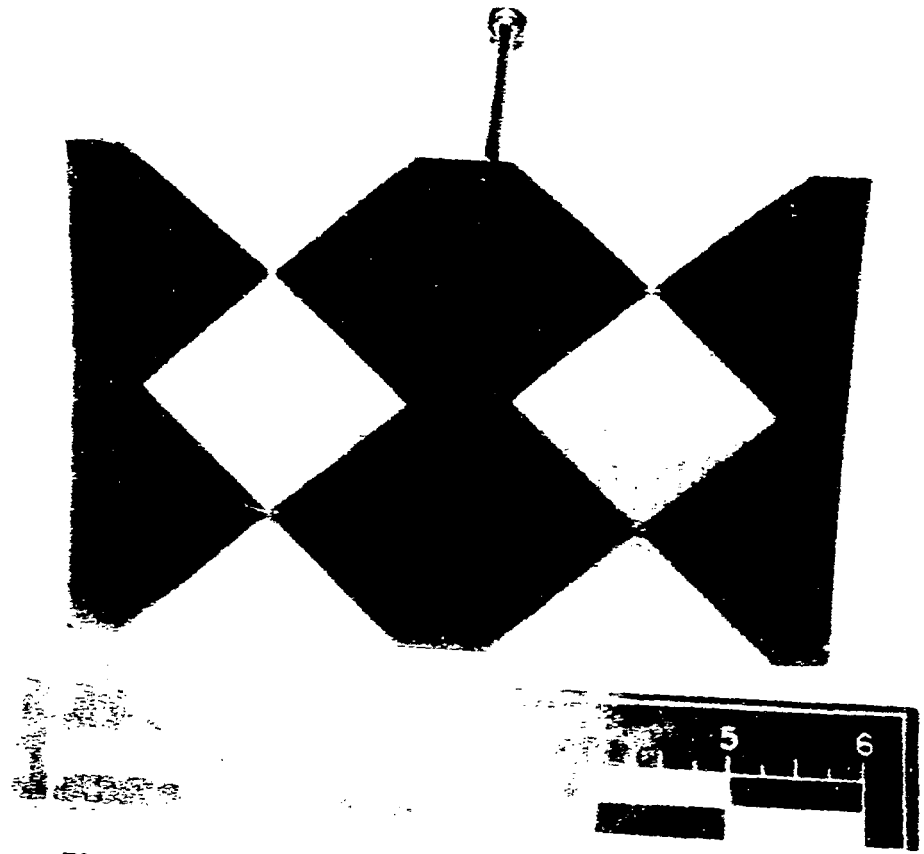

Figure 11. Circuit board of 1.75-in. diameter B dot sensor using microstrip feed.

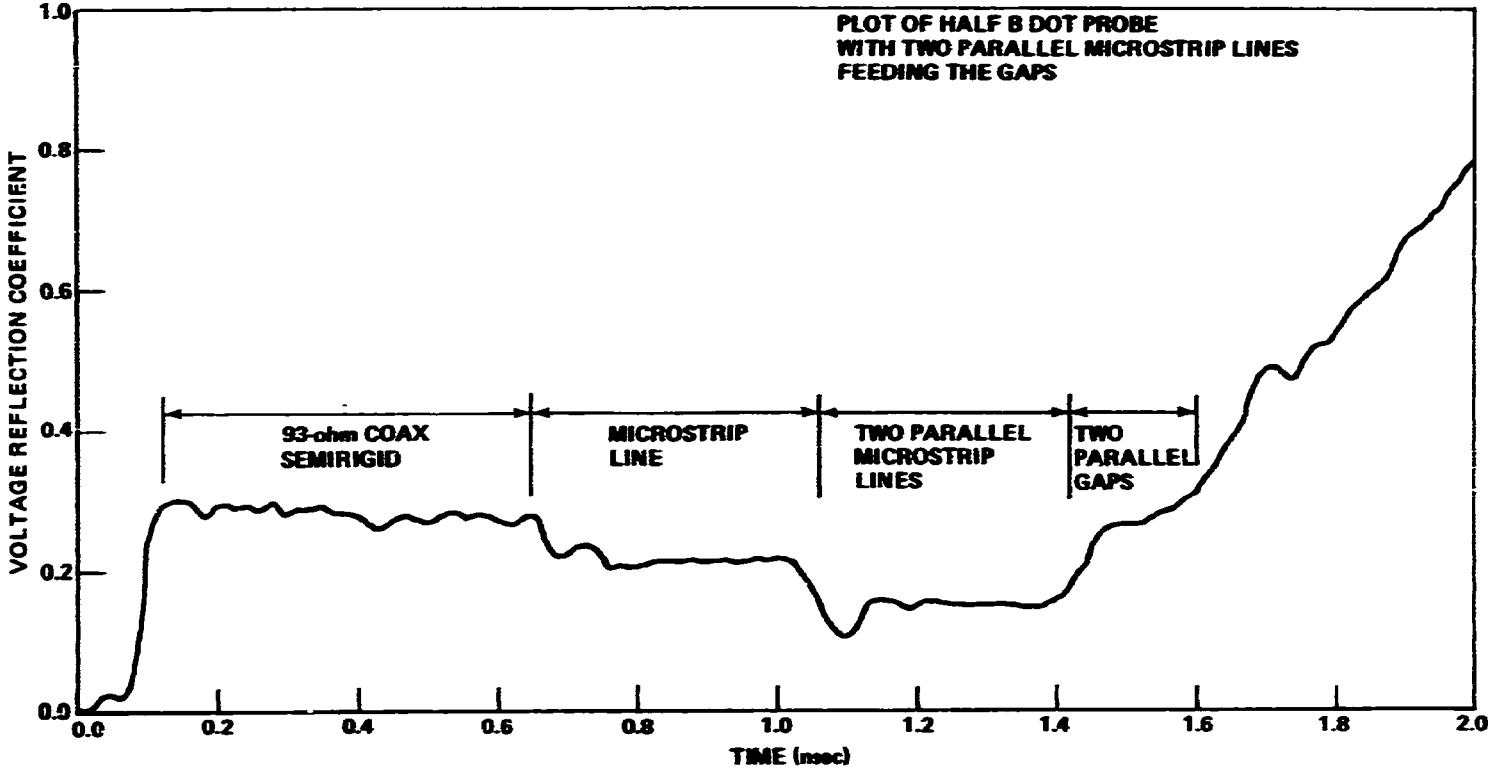

Figure 12. TDR measurement of unassembled 1.75-in. diameter B dot sensor with two parallel microstrip lines feeding a single gap at two points.

The double-gap probe was then assembled for impedance measurements. A partition was used along the 100-ohm coaxial cable to furnish a low inductance path to the electric field currents (Figures 13 and 14). A TDR plot of this double-gap probe is shown in Figure 15.

A second 1.75-in. diameter probe was fabricated without the 100-ohm section of microstrip, i.e., the 93-ohm cable junctions directly with two 200-ohm sections of microstrip. Next, a 7/8-in. diameter probe of the same configuration was assembled. This probe was built to increase the frequency response by halving the circumference and width dimensions of the 1.75-in. diameter probe (Figure 16).

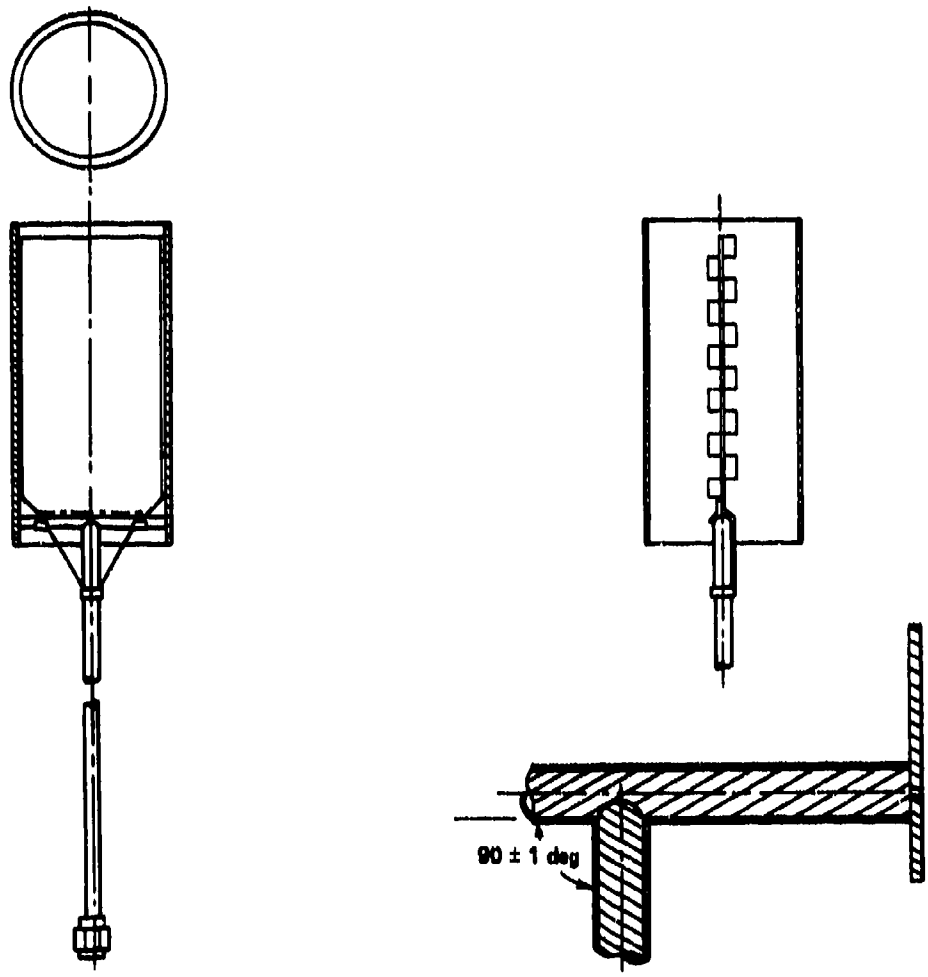

Figure 13. Assembled double-gap loop sensor with microstrip gap feeds.

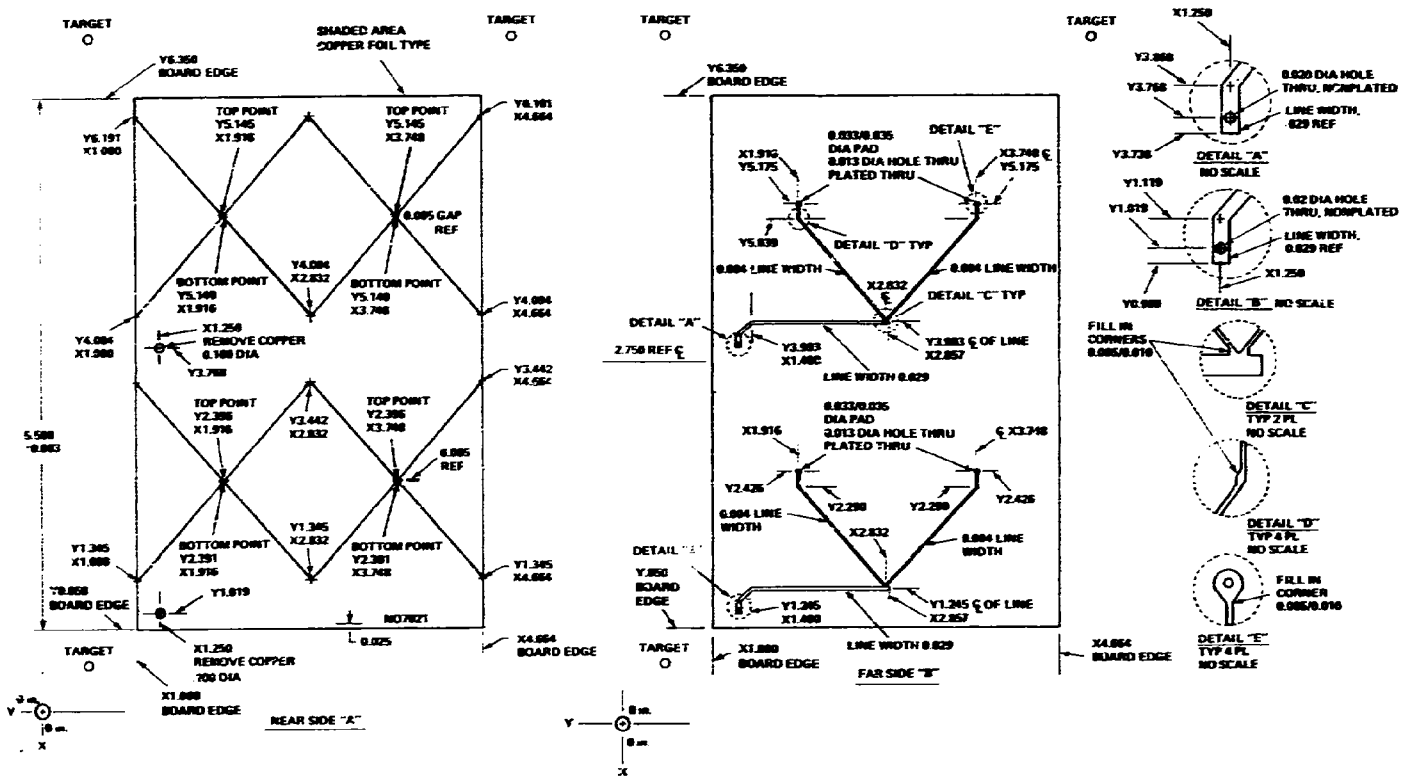

Figure 14. Circuit board drawing of 1.75-in. diameter B dot sensor.

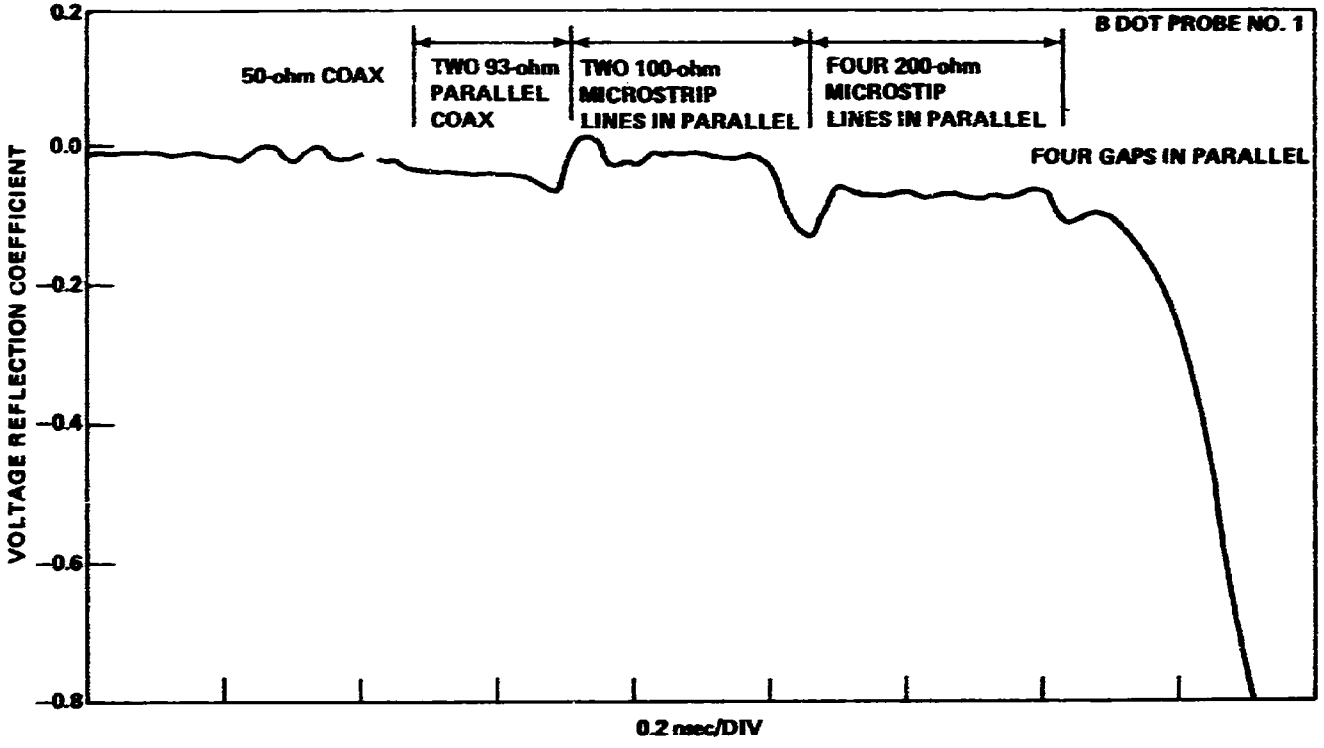

Figure 15. TDR measurement of 1.75-in. diameter B dot sensor using 100-ohm microstrip sections.

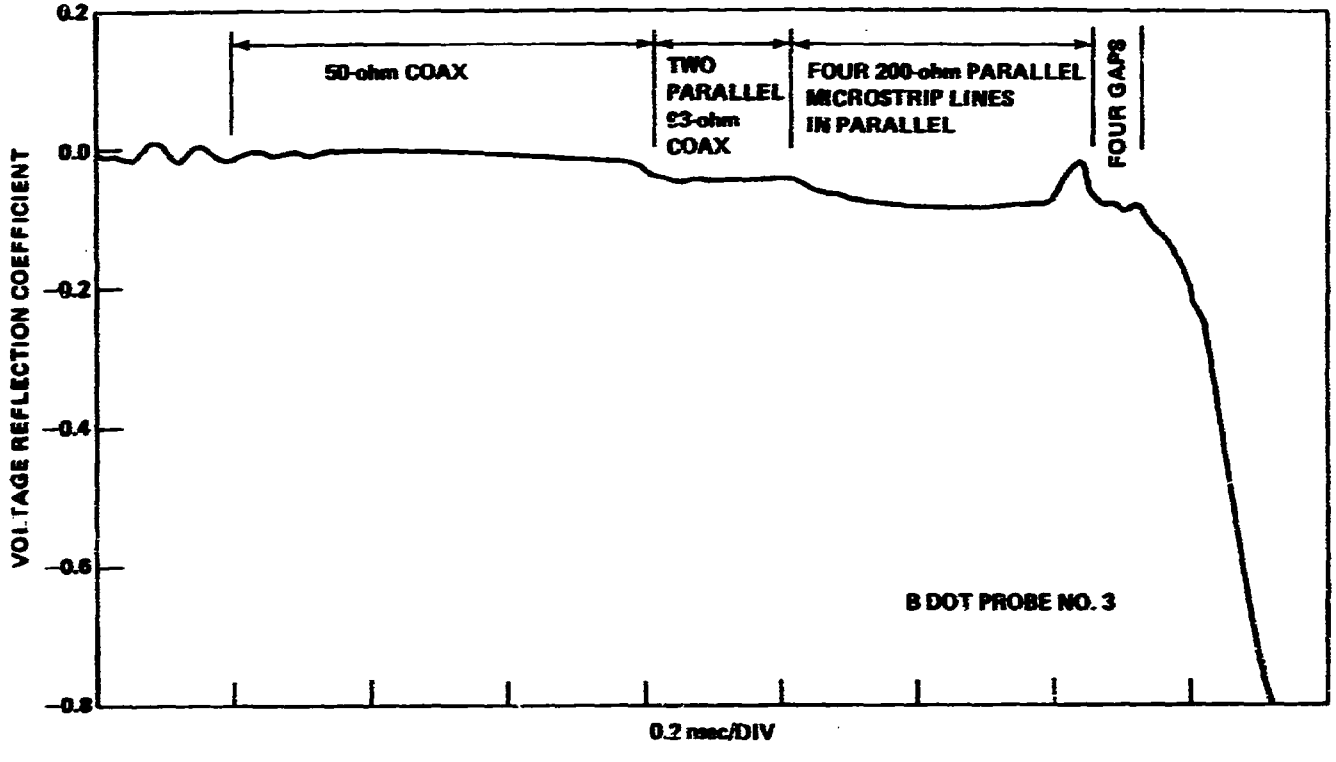

Figure 16. TDR measurement of 1.75-in. diameter B dot sensor without 100-ohm microstrip sections.

F. Far Field (Radiation) Patterns of a B Dot Probe

1. Anechoic Chamber

The facility utilized for the probe patterns was the NASA 120-ft chamber at Marshall Space Flight Center, Alabama. The chamber consists of a tapered section 90 ft long with a 30- × 30- × 30-ft working space for the antenna tower. The facility is shielded and has a pyramid-type absorber which reduces reflections by approximately 55 dB at 150 MHz to 65 dB at 2 GHz.

2. Test Configurations

The antenna tower is located approximately 100 ft from the transmitting antenna. The antenna pattern system is a Scientific Atlanta type consisting of a tower, rotator, receiver, and plotter. The probe was mounted on a vertical nonconductive rod and secured to the tower. The probe was then radiated by the test frequencies using a ridged horn driven by a RF communication 5-W tunable amplifier. The desired frequencies (150 to 500 MHz) for this set-up were generated by a Hewlett-Packard Model 8640B signal generator. Above 500 MHz, a Microdot power oscillator was used to drive the ridged horn.

3. Radiation Patterns

The measured patterns are shown in Figures 17, 18, and 19. From these patterns it is obvious that certain abnormalities developed as the frequency increased beyond the normal operating frequency of the probe as explained in Section II.B. Slight abnormalities do not preclude the use of the probe, provided it is calibrated against a suitable standard. Therefore, based on the uniformity of patterns, the 1.75-in. probe can be calibrated and used with confidence up to 1 GHz. A narrowing of the pattern makes the orientation of the probe more critical, and reduced output at the higher frequencies only changes the calibration factor. As the frequency of the field is increased higher than the normal operating frequency limit, the patterns begin to break up and cause the probe to have several nulls making it difficult to calibrate and use.

III. TECHNIQUE FOR ESTABLISHING KNOWN STANDARD ELECTROMAGNETIC FIELDS USING NBS STANDARD DIPOLES

A. Standard-Antenna Calibration Method for Dipoles

The standard antenna procedure for calibrating horizontally-polarized antennas from 30 MHz to 1 GHz is accomplished by using the NBS standard dipoles to set up an accurately known electromagnetic field [8]. The dipole is usually mounted 8 to 10 ft above the

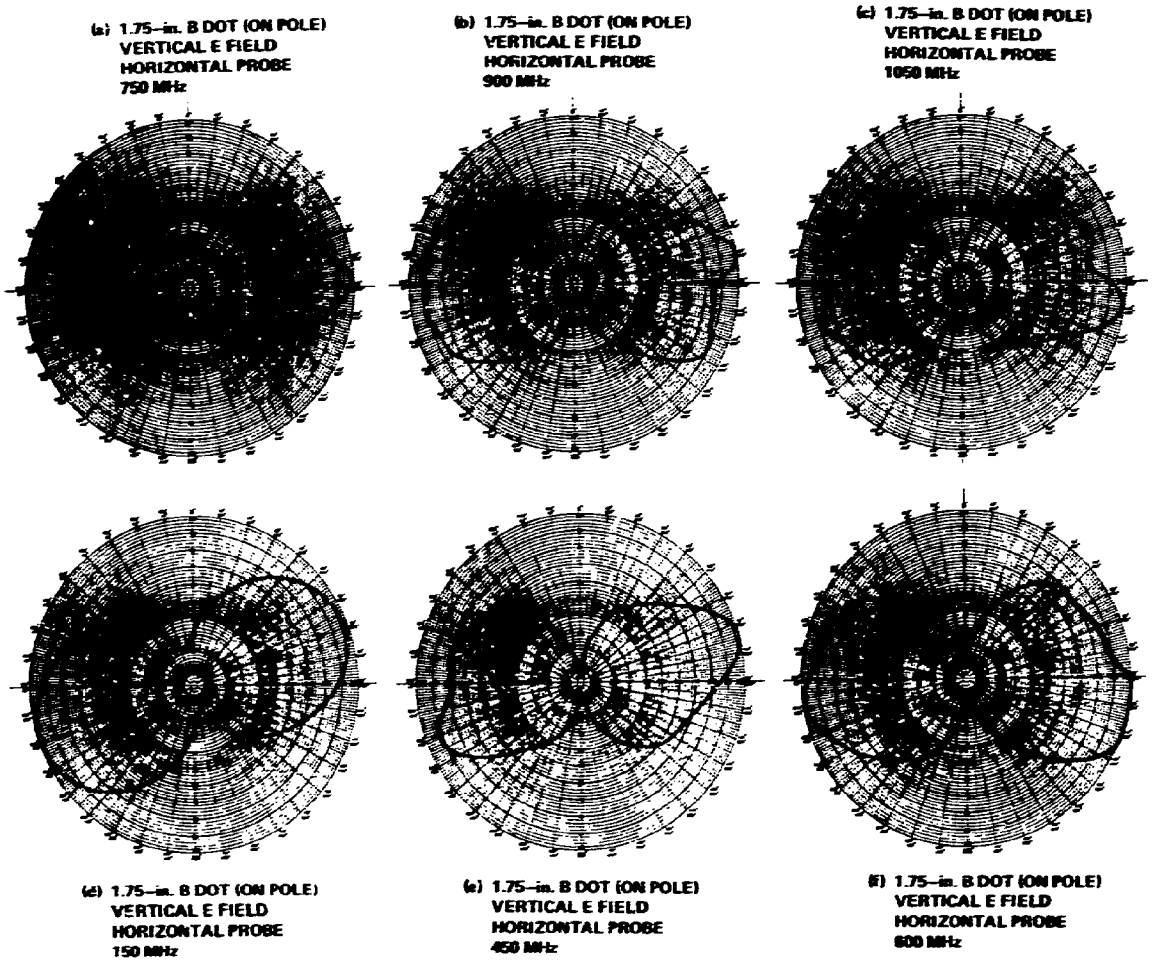

Figure 17. 1.75-in. diameter B dot probe antenna patterns.

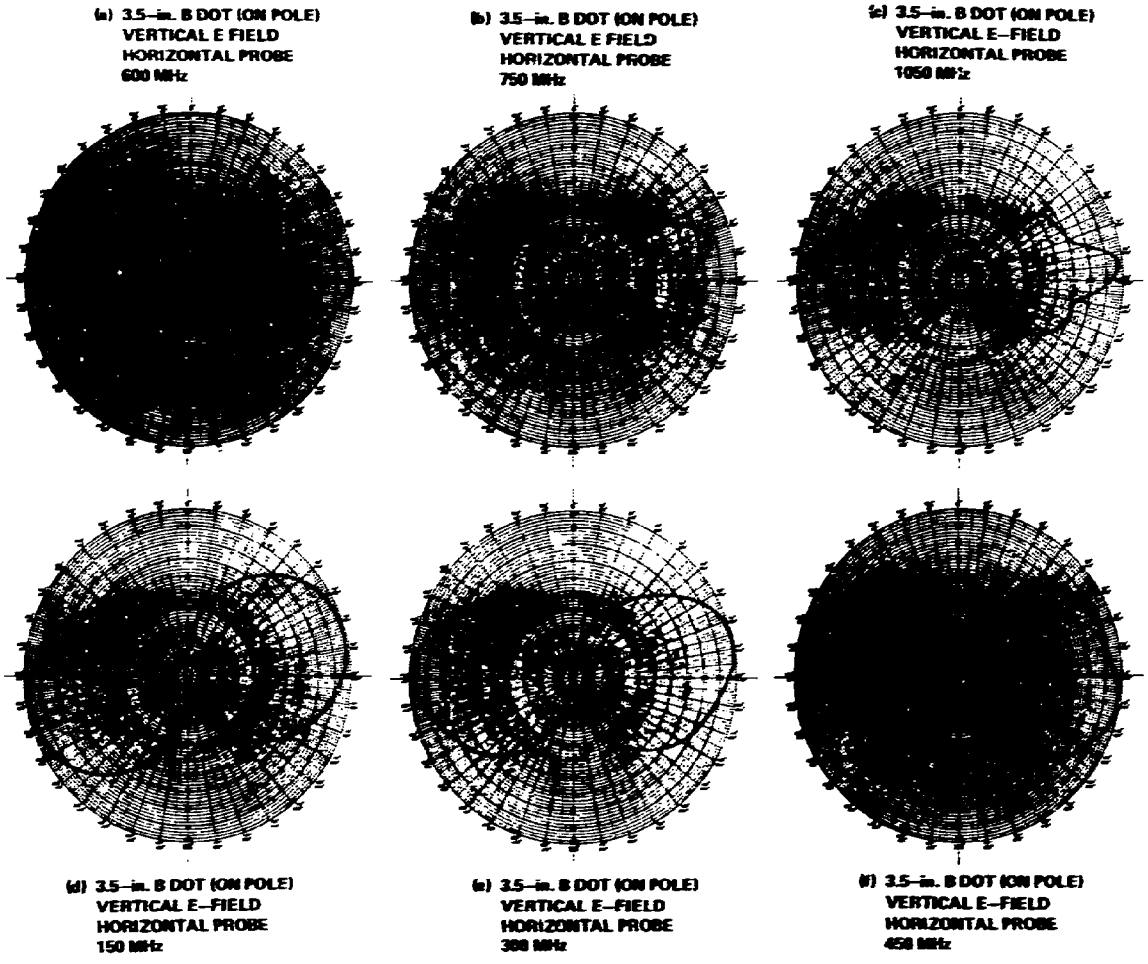

Figure 18. 3.5-in. diameter B dot probe antenna patterns.

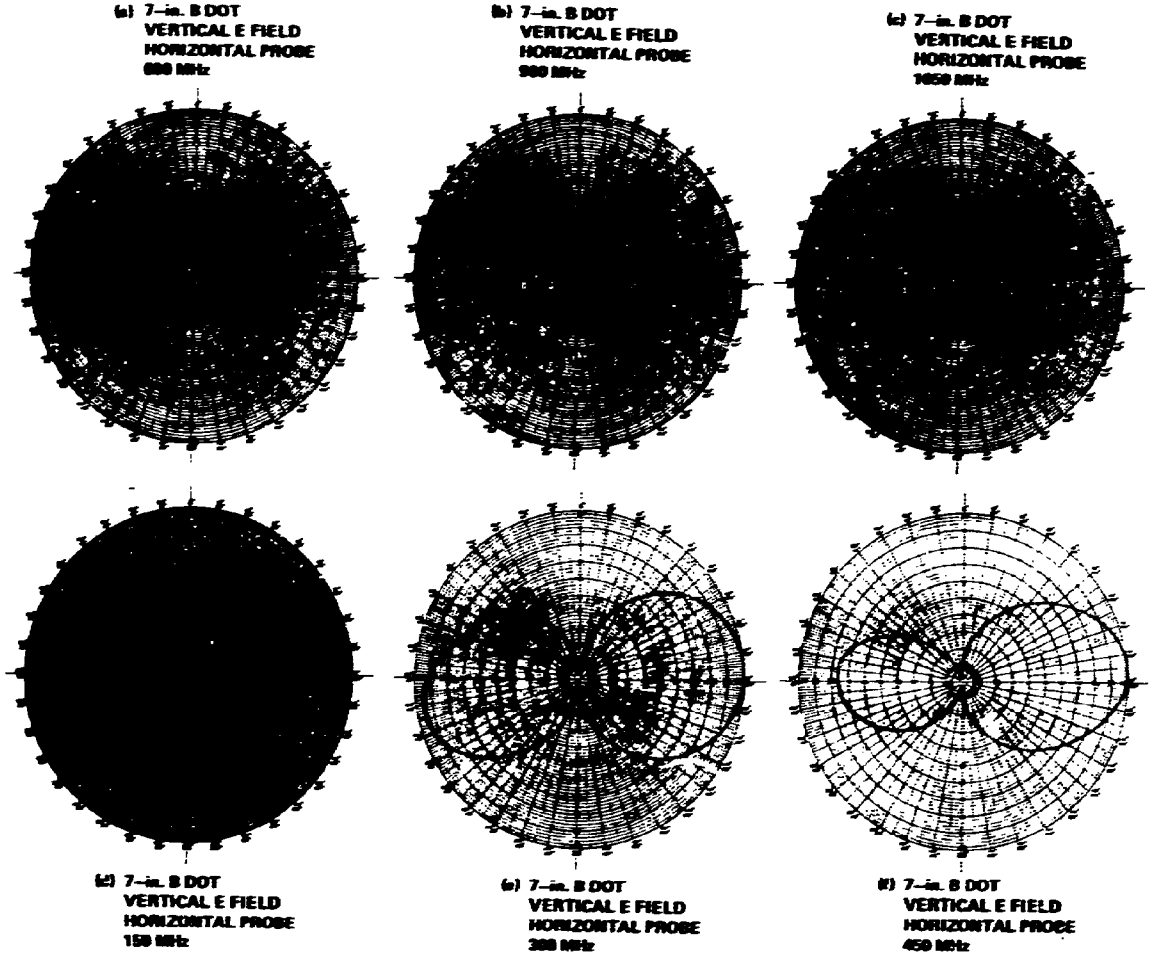

Figure 19. 7-in. diameter B dot probe antenna patterns.

ground. Care must be taken to assure that the field is steady, i.e., there are no transmitting level changes. The antenna to be calibrated is then substituted for the standard antenna, and the antenna coefficient is determined. The coefficient is given by

$$C = \frac{E_s}{E_t} \quad , \tag{15}$$

where

C = the antenna coefficient

E_s = the standard field, V/m

E_t = the field measured by the test antenna, V/m.

The standard antennas are comprised of a self-resonant half-wave antenna, with a high impedance-balanced voltmeter at the center of the dipole. The balanced voltmeter is composed of a selected point contact silicon crystal diode detector with a RC filter network. The output of the detector can be read by any high impedance digital millivolt meter. Figure 20 shows the 300-MHz to 1-GHz standard antenna. The upper mount of the antenna is made of polytetrafluorethylene (PTFE). The elements are 1/16-in. diameter rods with the ends threaded to allow for changing the operating frequency of the antenna.

The next important consideration is the selection of a suitable diode detector. The diode output should be as flat as possible over the desired frequency range. The detector should not be temperature sensitive. After evaluating several types of detectors, the NBS recommends a ceramic cartridge-type for 30 to 400 MHz and selected-type, glass-incapsulated, subminiature for 300 MHz to 1 GHz.

B. Calibration of Diodes

The frequency response of the detector diode used must be evaluated very accurately prior to making field measurements. The set-up recommended by NBS is shown in Figure 21. The low pass filter eliminates generator harmonics. The 20-dB attenuator serves to isolate the generator. The mount used by NBS is a modified N-Type T-Connector. A cut-away view is shown in Figure 22. The filtering of the output of the detector is accomplished by the approximately 100 pF which is formed by the connector body and the brass cylinder which holds the upper portion of the diode. The cylinder and the connector body are insulated by 2 mils of PTFE tape. There are adapters for calibrating either type diode. The voltage standing wave ratio of this mount has been found to be less than 1.05 up to 1 GHz. Typical response curves for the two recommended type diodes are shown in Figure 23. These curves are of selected diodes and are not representative of all diodes.

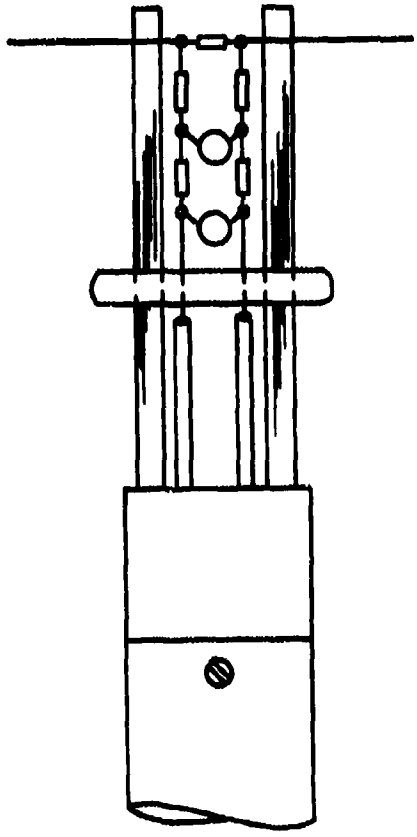

Figure 20. 300-MHz to 1-GHz NBS standard antenna.

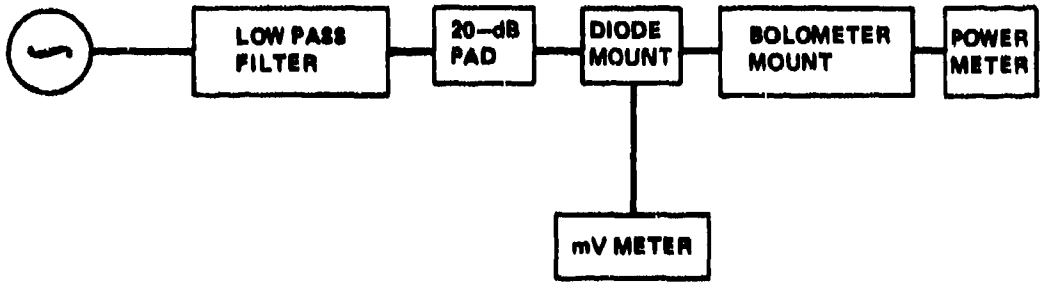

Figure 21. Diode calibration set-up.

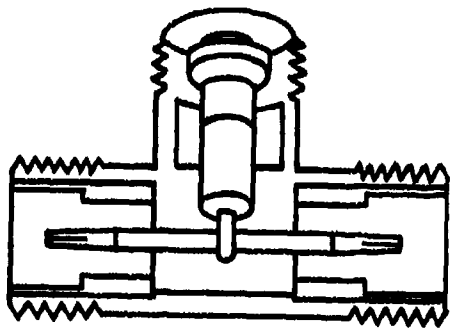

Figure 22. Cut away view of diode frequency response mount.

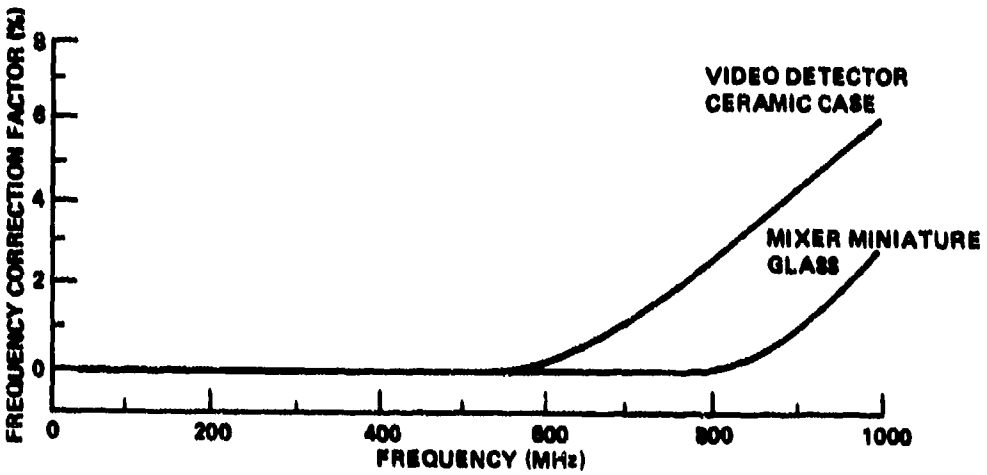

Figure 23. Frequency response curves for selected diodes.

It can readily be seen that the ceramic diodes are flat to approximately 500 MHz and would be suitable for the lower frequencies (30 to 400 MHz). The glass-type diodes are flat to approximately 800 MHz with normally no more than 4% correction for the higher frequencies (1 GHz). NBS has evaluated temperature coefficients of both types of diodes and found that these coefficients are not uniform, i.e., some outputs go up as temperature increases, but most of them decrease. This makes it desirable to calibrate at a temperature which is near the temperature of the test field. If this is not possible, temperature corrections can be added. The crystal detectors are now ready to be calibrated as balanced RF voltmeters. They are placed in the center of the standard dipoles, and a 150-mV 50-MHz RF source is applied across the diode as shown in Figure 24. The output of the detector is read on a digital

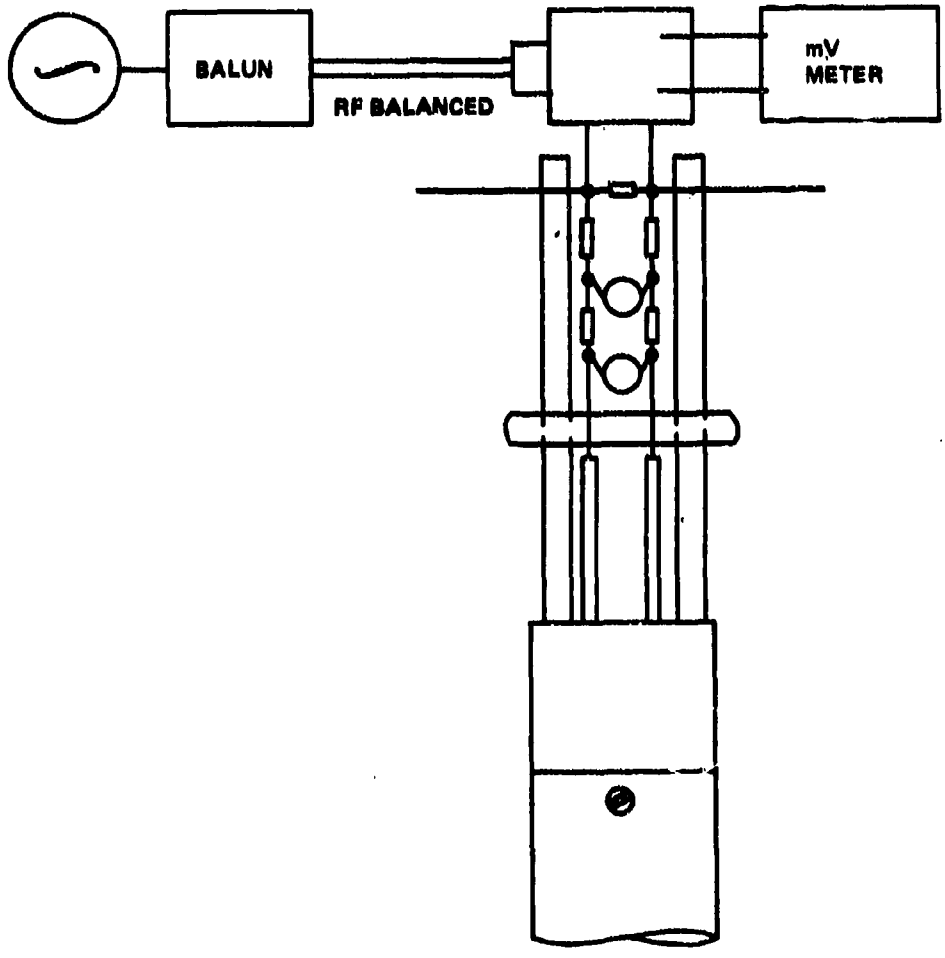

Figure 24. Balanced voltage standard connected to standard NBS antenna.

millivolt meter and recorded. The voltage across the diode is reduced by a step attenuator and the output of the detector recorded. A graph of RF voltage versus dc output is then plotted. One now has an accurately calibrated balanced millivoltmeter.

C. Analysis of Reduced Dipole Voltage

The induced voltage in a resonant half-wave dipole can be expressed in terms of its resonant length. If a sinusoidal current

distribution is assumed, the following relationship is obtained:

$$\ell_{eff} = \frac{\lambda}{\pi} \tan \frac{\pi \ell}{\lambda} \quad ,$$

where ℓ is the antenna half-length in meters and λ is the wavelength.

For a half-wave self-resonant dipole, $\ell_{eff} = \lambda/\pi$. Since the induced voltage is measured by a high impedance balanced RF voltmeter, it is the same as the open circuit voltage. This allows one to use the following relationship to determine the magnitude of the E field

$$|E| = \frac{V_{oc}}{\ell_{eff}} \quad , \tag{17}$$

where

$|E|$ = electric field (V/m)

V_{oc} = open circuit voltage (V)

ℓ_{eff} = the antenna effective length.

D. Details of the Construction of a Self-Resonant Half-Wave Dipole

To construct a self-resonant half-wave dipole with a finite thickness, the length is shortened as a function of antenna rod size and frequency. The amount of shortening is given by the following relationship [8]:

$$\% \text{ shortening} = \frac{2708}{K_o} \quad , \tag{18}$$

where

$$K_o = 120\left[\log_e\left(\frac{\lambda}{d}\right) - 1\right]$$

d = antenna rod diameter (cm).

The percent shortening is normally no more than 6%, depending on the diameter to length ratio.

The transmitting and receiving antennas should be more than 3λ apart, which is approximately 100 ft for the 30 to 400 MHz and 40 ft for the 400 MHz to 1 GHz. The antennas are mounted approximately 10 ft above the ground. The ground has little effect on the antenna impedance and the resulting antenna coefficient.

IV. FIELD CALIBRATION OF THE B DOT PROBES

A. Initial Calibration for Determining Loop Equivalent Area

If a uniform plane wave in free space is X polarized and travels in the positive Z direction according to the coordinate system shown, the traveling wave has the following components:

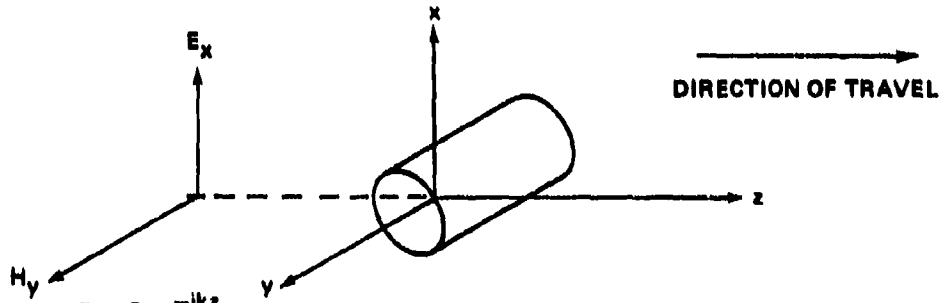

$$E_x = E_0 e^{-jkz}$$

$$H_y = \frac{E_0}{\eta} e^{-jkz}$$

where

$$k = \omega\sqrt{\mu_0 \epsilon_0} = \omega/c$$

$$\eta = \sqrt{\mu_0/\epsilon_0}$$

The time-varying flux density, with the origin colocated with a cylindrical loop probe, may be expressed as:

$$B_y = \mu_0 H_y = \frac{\sqrt{2}E_0}{c} \cos \omega t \quad . \tag{19}$$

From Equation (2) the voltage (V_p) across a single-gap cylindrical loop oriented in the manner shown is

$$V_p = -A_{eq} \frac{d B_y}{dt} = A_{eq} \frac{\omega E_0}{c} \sin \omega t$$

$$|V_p| = \frac{2\pi A_{eq} E_0 f}{c} \quad . \tag{20}$$

The geometrical area of the loop sensor may be used in Equation (20) if the probe is assumed to be 100% efficient over some frequency band of operation. The equivalent area may be calculated from measured probe voltages at discrete frequencies while holding a known field strength.

The response of two sizes of single-gap and double-gap B dot loop sensors were plotted from experimental data taken in a known continuous wave electromagnetic field of 20 V/m. A block diagram of the equipment used for the field measurements is shown in Figure 25. The ridged horns used are of the type discussed by Karr [9,10]. A photograph of the equipment used in the test setup is shown in Figure 26. The loop dimensions of the two single-gap probes used for comparative measurements are shown in Figure 27. TDR plots of the two single-gap probes are shown in Figures 28 and 29.

Rearranging the equation for probe voltage [Equation (20)], and solving for the area (A_{eq}) gives

$$A_{eq} = \frac{c\ V_p}{2\pi\ f\ E_0} \quad . \tag{21}$$

In the test setup, a constant electric field (E_0) is applied at many frequencies from 32 MHz to 2.5 GHz. The voltage output of the probe cable is measured at each test frequency. This voltage is corrected for the cable losses to obtain the output voltage of the probe (V_p). The V_p is plotted on the y-axis and the frequency is plotted on the x-axis. From this plot, V_p and E_0 can be used to determine the electrical effective area (A_{eq}).

The effective geometrical area of the B dot loop is calculated by using the probe area minus any blockage by cables and partitions inside the loop. The double-gap loop is effectively a half-turn loop and thus the area must be halved. The 1.75-in. and 0.875-in. double-gap loops had 0.130-in. diameter 93-ohm semirigid coaxial cable across the loop diameter. Since the cable obstructions are cylindrical, it was believed that approximately half the energy hitting the cable surface would be reflected and half would be scattered through the loop. Therefore, one half of the cable length times the cable diameter was subtracted from the total loop area.

The raw data from the probe calibration procedure contain random data measuring errors. This type of error can be reduced by applying statistical techniques. The technique used in this case is linear regression, and the following basic concepts of this approach are summarized from references 9 and 10, Draper and Smith [11], and Ostle [12]. First, the following quantities must be defined:

a) $y = a_0 + a_1 X$,

where a_0 is the intercept and a_1 is the slope (the fit is obtained by the least squares method).

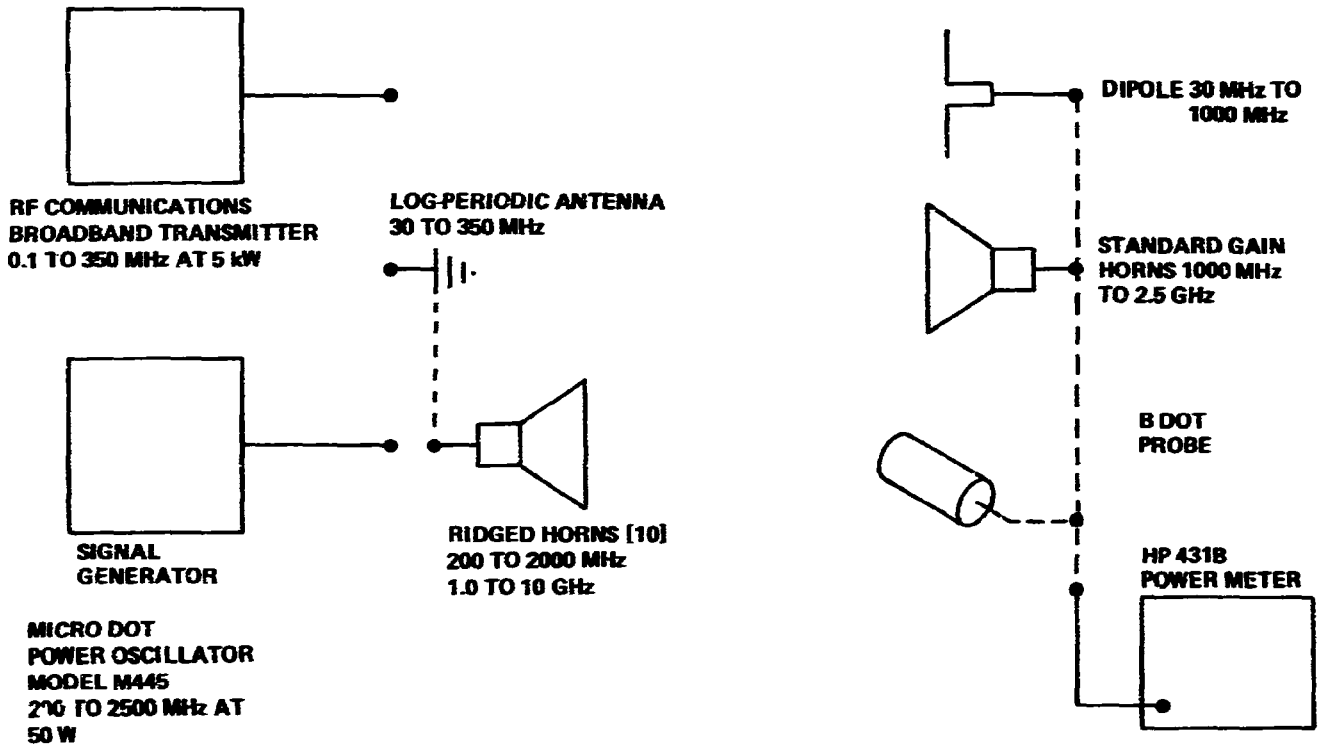

Figure 25. Block diagram of equipment used to obtain calibration data for B dot loop sensor.

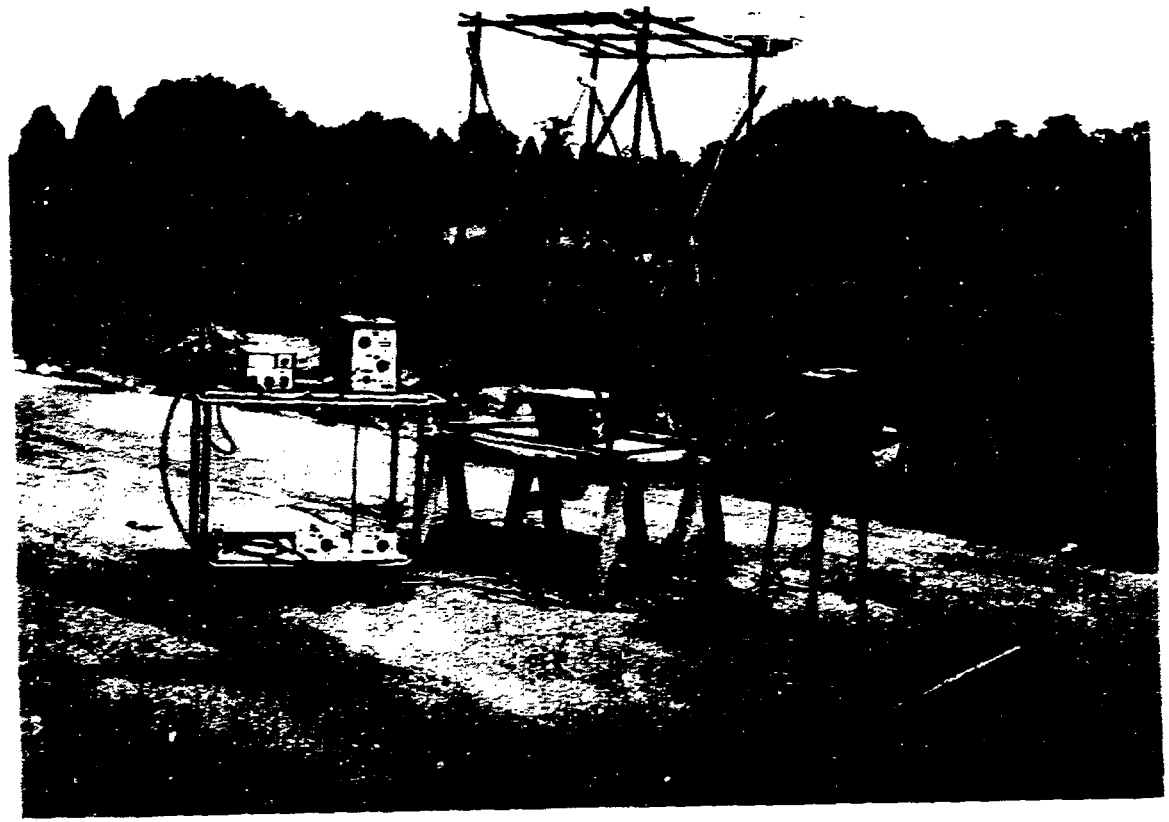

Figure 26. Equipment used for sensor calibration measurements.

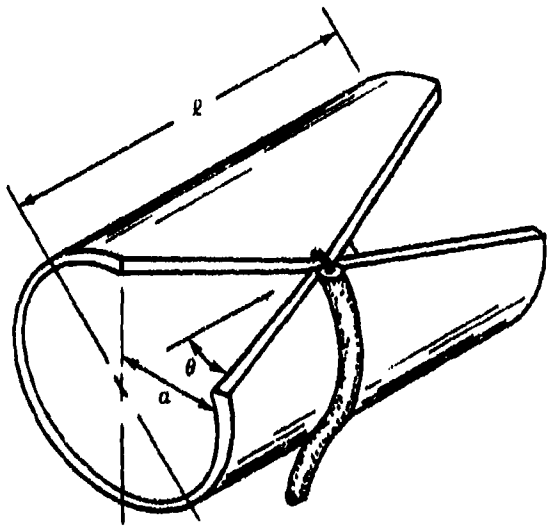

SINGLE GAP LOOP
B DOT PROBE

	2a (in.)	ℓ (in.)	θ (deg)
MODEL 1	1.75	1.75	14
MODEL 2	1.00	1.00	11

Figure 27. Single-gap loops used for comparative measurements to double-gap loop B dot sensors.

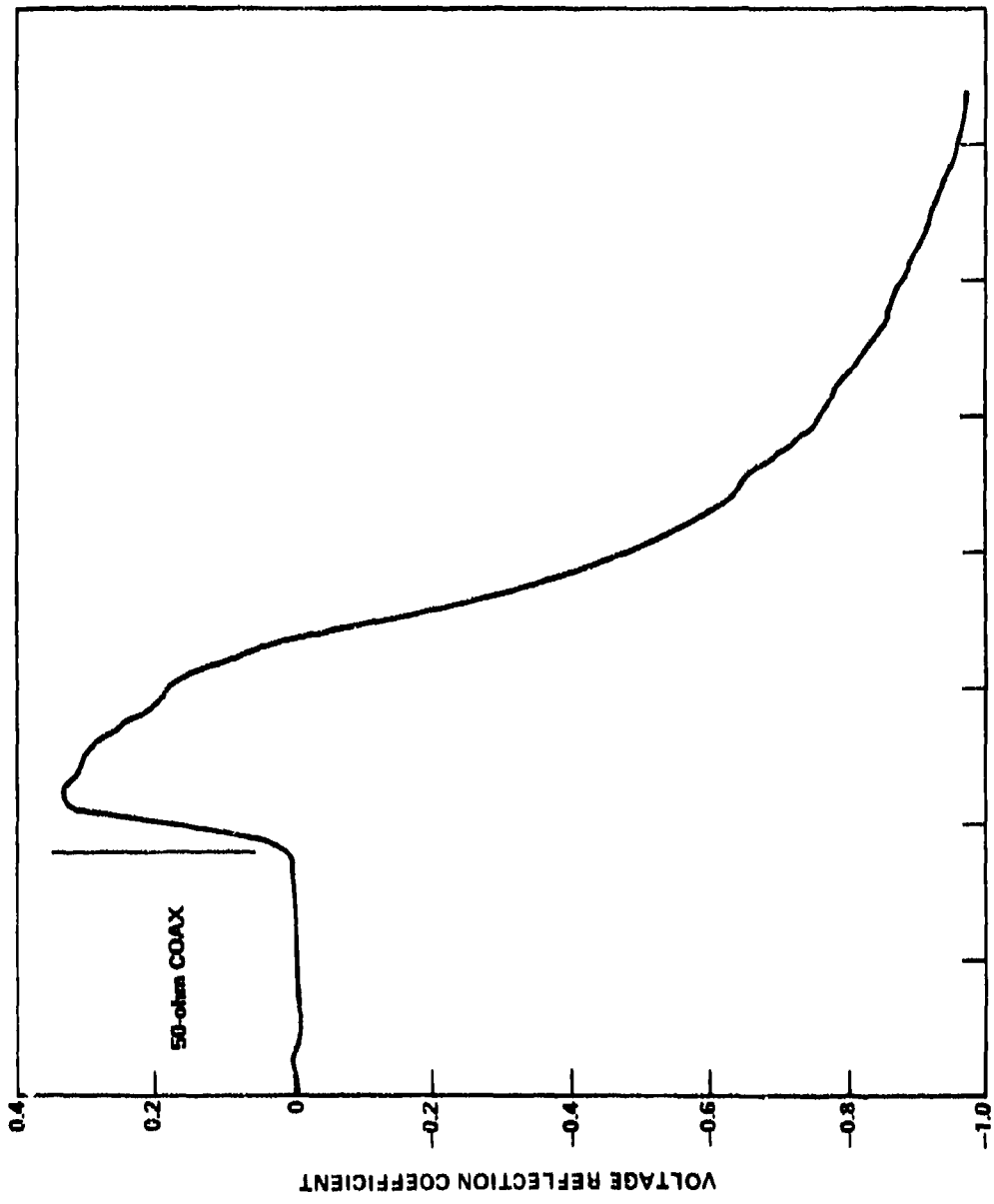

Figure 28. TDR plot of single-gap B dot probe (1.0-in. diameter).

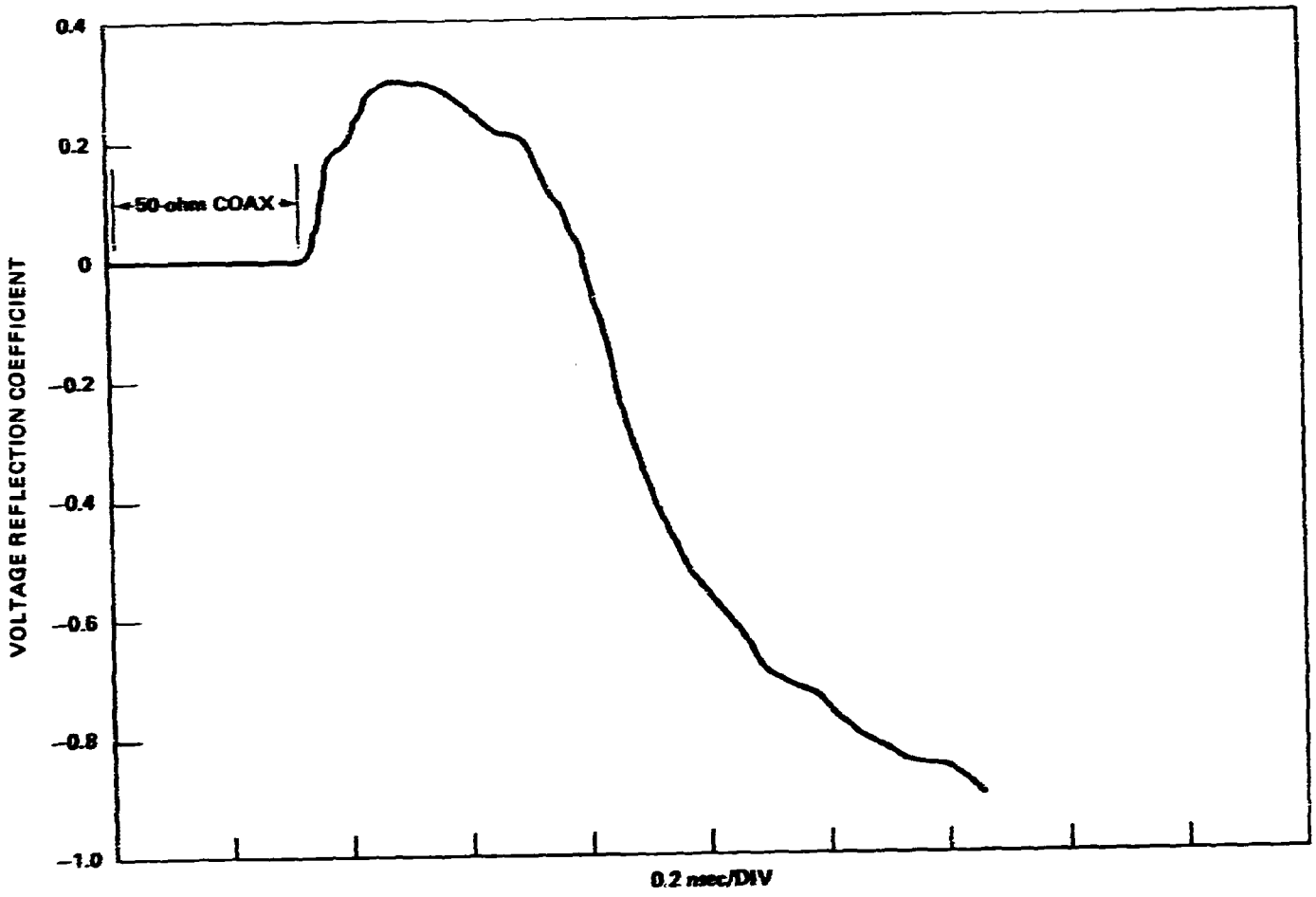

Figure 29. TDR plot of single-gap B dot probe (1.75-in. diameter).

b) Regression coefficients a_0, a_1:

$$a_1 = \frac{\Sigma x_i y_i - \frac{\Sigma x_i \Sigma y_i}{n}}{\Sigma x_i^2 - \frac{(\Sigma x_i)^2}{n}}$$

$$a_0 = \bar{y} - a_1 \bar{x}$$

$$\bar{x} = \frac{\Sigma x_i}{n}$$

$$\bar{y} = \frac{\Sigma y_i}{n}$$

c) Coefficient of determination:

$$r^2 = \frac{\left[\Sigma x_i y_i - \frac{\Sigma x_i \Sigma y_i}{n}\right]^2}{\left[\Sigma x_i^2 - \frac{(\Sigma x_i)^2}{n}\right]\left[\Sigma y_i^2 - \frac{(\Sigma y_i)^2}{n}\right]} ,$$

where r^2 measures how well the points fit the regression line (note $0 \leq r^2 \leq 1$; and if $r^2 = 1$, one has a perfect fit).

d) Estimated value y on the regression line for any given x:

$$y = a_0 + a_1 x .$$

e) Standard error of estimate of y on x:

$$s_{y \cdot x} = \left[\frac{\Sigma(y_i - \hat{y}_i)^2}{n - 2}\right]^{1/2} = \left[\frac{\Sigma y_i^2 - a_0 \Sigma y_i - a_1 \Sigma x_i y_i}{n - 2}\right]^{1/2} .$$

f) Standard error of the regression coefficient a_0:

$$s_0 = s_{y \cdot x} \left[\frac{\Sigma x_i^2}{n\left[\Sigma x_i^2 - \frac{(\Sigma x_i)^2}{n}\right]}\right]^{1/2} .$$

g) Standard error of the regression coefficient a_1:

$$S_1 = \frac{y \cdot x}{\left[\sum x_i^2 - \frac{\left(\sum x_i\right)^2}{n}\right]^{1/2}} \quad .$$

Note: n is a positive integer, and n = 1 or 2.

The linear regression line can now be used to determine the best estimate of the equivalent area (A_{eq}) of the probe, and the calculated area based on the measured E_0 and V_p can be compared with the actual geometric area of the probe to determine the percent efficiency of the probe.

$$\frac{A_{eq} \times 100}{A \text{ geometrical}} = \text{percent efficiency (PE)} \quad . \qquad (22)$$

Linear regressions are computed for selected upper frequency limits and the percent efficiency determined. The upper frequency limit to which the probe can be used is then determined by the maximum error one can tolerate in the E-field measurement. A departure from the theoretical line occurs as the field exceeds the high frequency limits of the probe such that V_p at specific frequency points is much less than calculated for the given probe area. Table 1 shows the comparison between the geometrical area and the equivalent area up to the point that the output of the probe deviates significantly from the calculated values. Above this point the deviation of measured single point frequency data were compared to calculated values.

Figures 30 through 33 display the measured data along with the theoretical values represented by the diagonal line passing through the origin. Table 2 presents the results of the linear regressions, equivalent area calculations (A_{eq}), and percent error calculations (%E) for the two single-gap and two multi-gap B dot probes.

The regression equation for the 1-in. single-gap B dot sensor output as presented in Table 2 is $V_p = a_0 + a_1 f$. Voltage calculation for the 650-MHz regression is as follows:

$$V_p = 0.4566 \text{ mV} + 0.2022 \text{ mV/MHz} \times 650 \text{ MHz} = 131.\text{?} \text{ mV at 650 MHz.}$$

This linear regressed line is shown as a dotted line on Figure 25.

TABLE 1. COMPARISON OF SENSOR LINEAR REGRESSED EQUIVALENT AND GEOMETRICAL AREAS

Probe Tested	Equivalent Area (m^2)	Geometrical Area (m^2)	Probe Response					
			dB	Frequency (MHz)	dB	Frequency (MHz)	dB	Frequency (MHz)
Single gap								
1-in. diameter	4.83×10^{-4}	5.07×10^{-4}	-0.43	32-650	-3	890	-3.9	1300
1.5-in. diameter	9.33×10^{-4}	1.14×10^{-3}	-1.74	32-650	-3	690	-5.3	1300
Double gap								
7/8-in. diameter	1.85×10^{-4}	1.76×10^{-4}	-0.43	32-2500	—	—	—	—
1.75-in. diameter	6.92×10^{-4}	7.39×10^{-4}	-0.57	32-1150	-1.1	1600	-0.69	2500

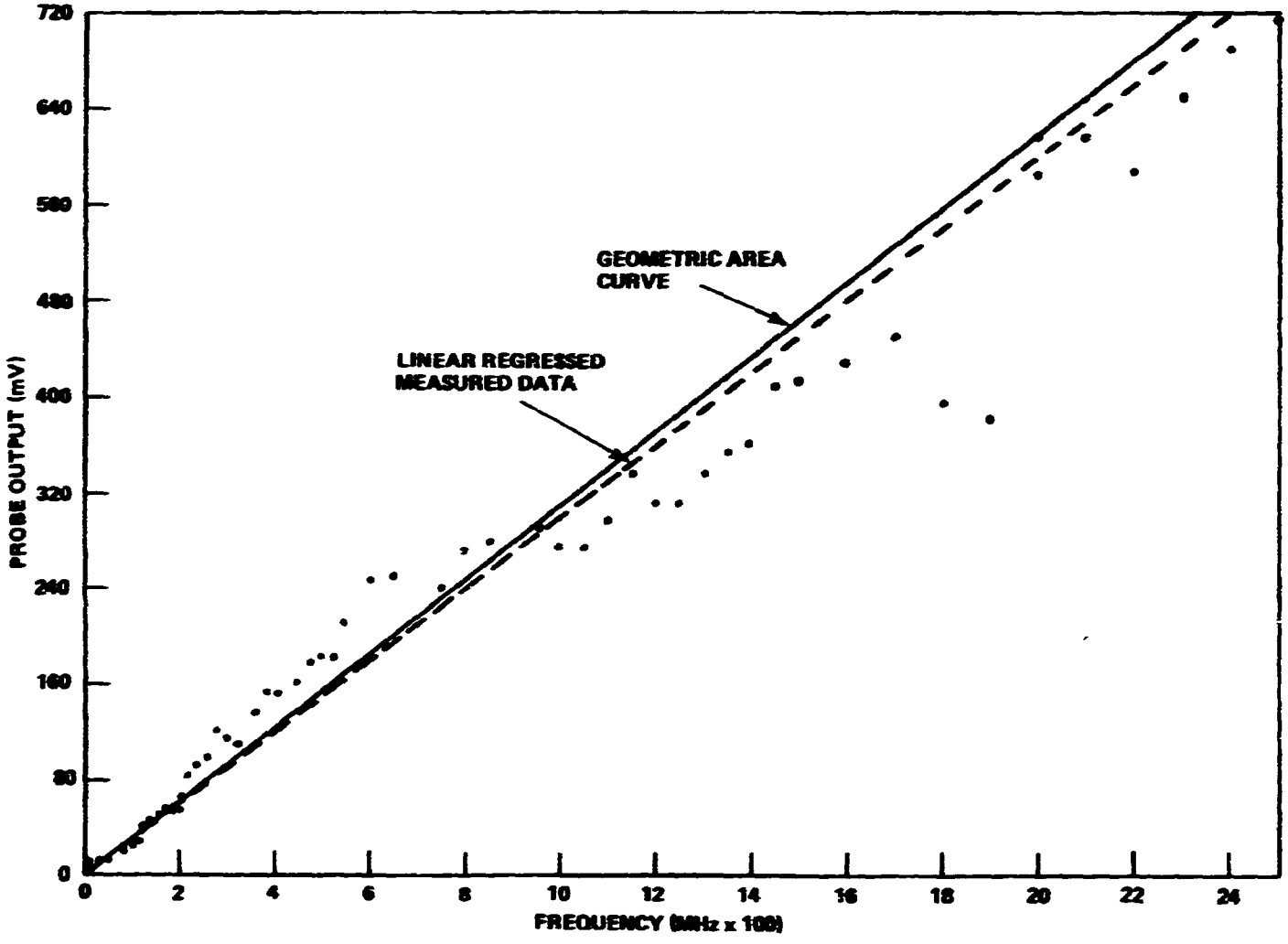

Figure 30. Calibration curve for 1.75-in. double-gap B dot loop sensor, E_0 = 20 V/m.

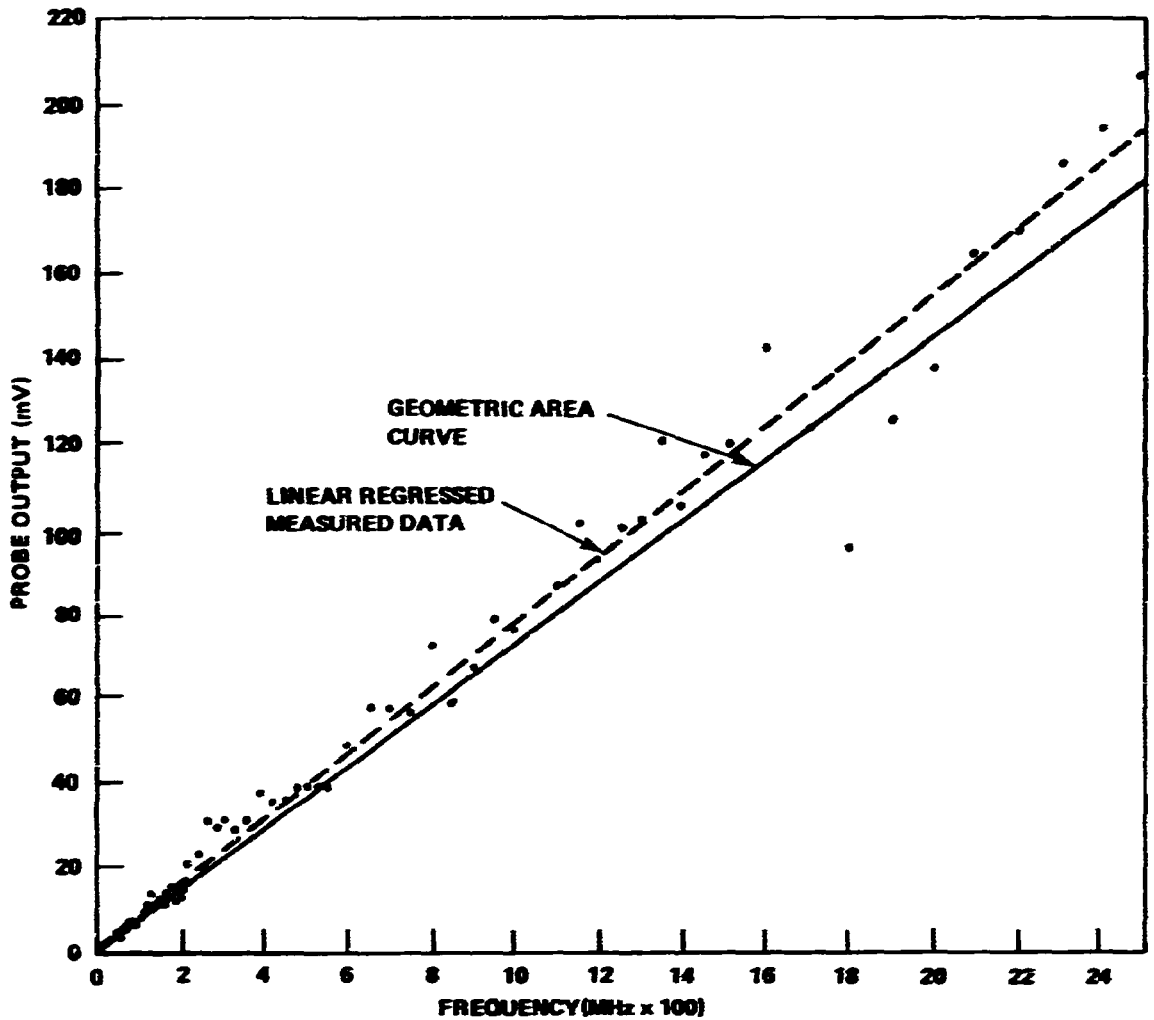

Figure 31. Calibration curve for 7/8-in. double-gap B dot sensor, E_0 = 20 V/m.

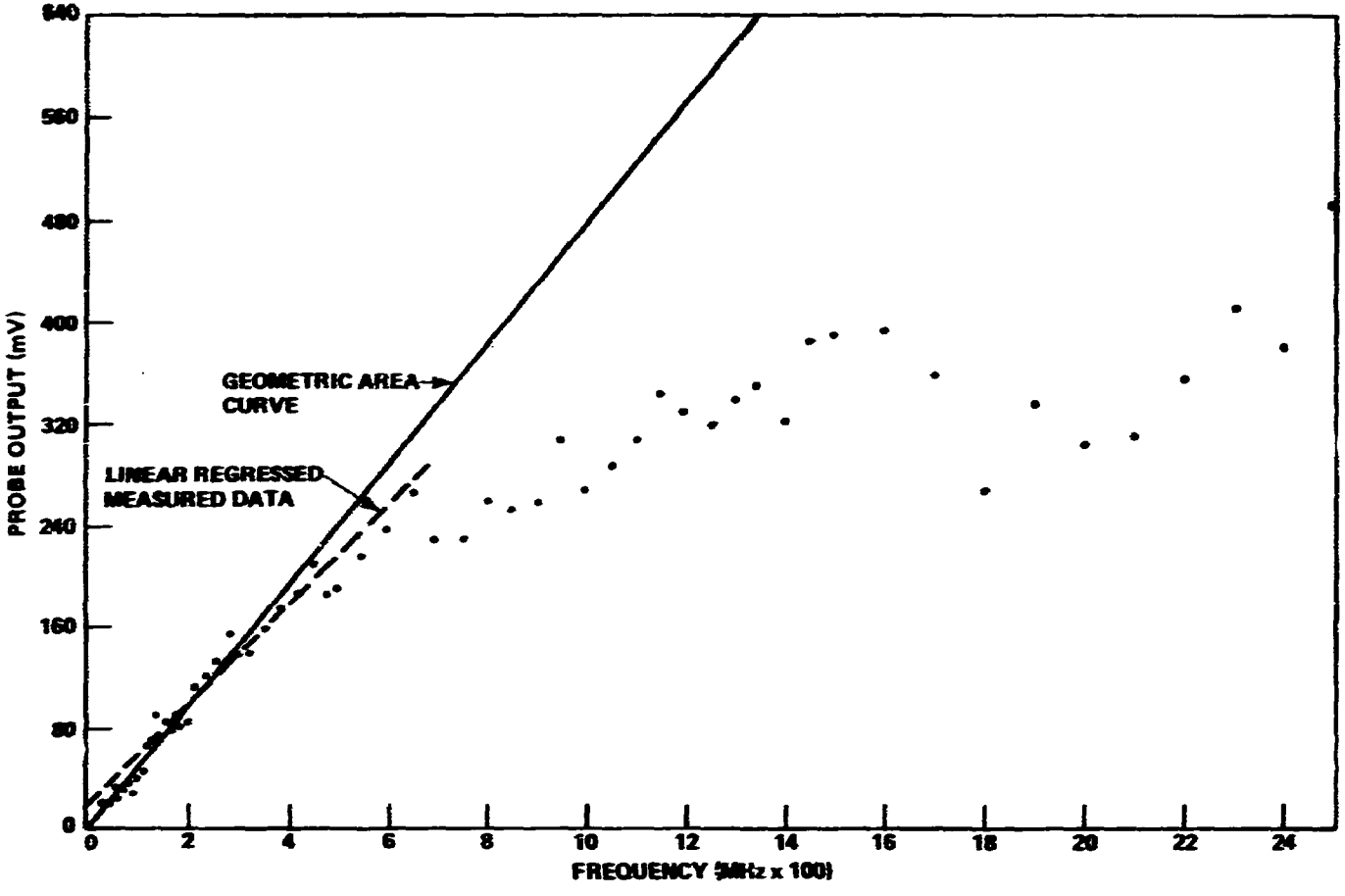

Figure 32. Calibration curve for 1.5-in. single-gap B dot sensor, E_0 = 20 V/m.

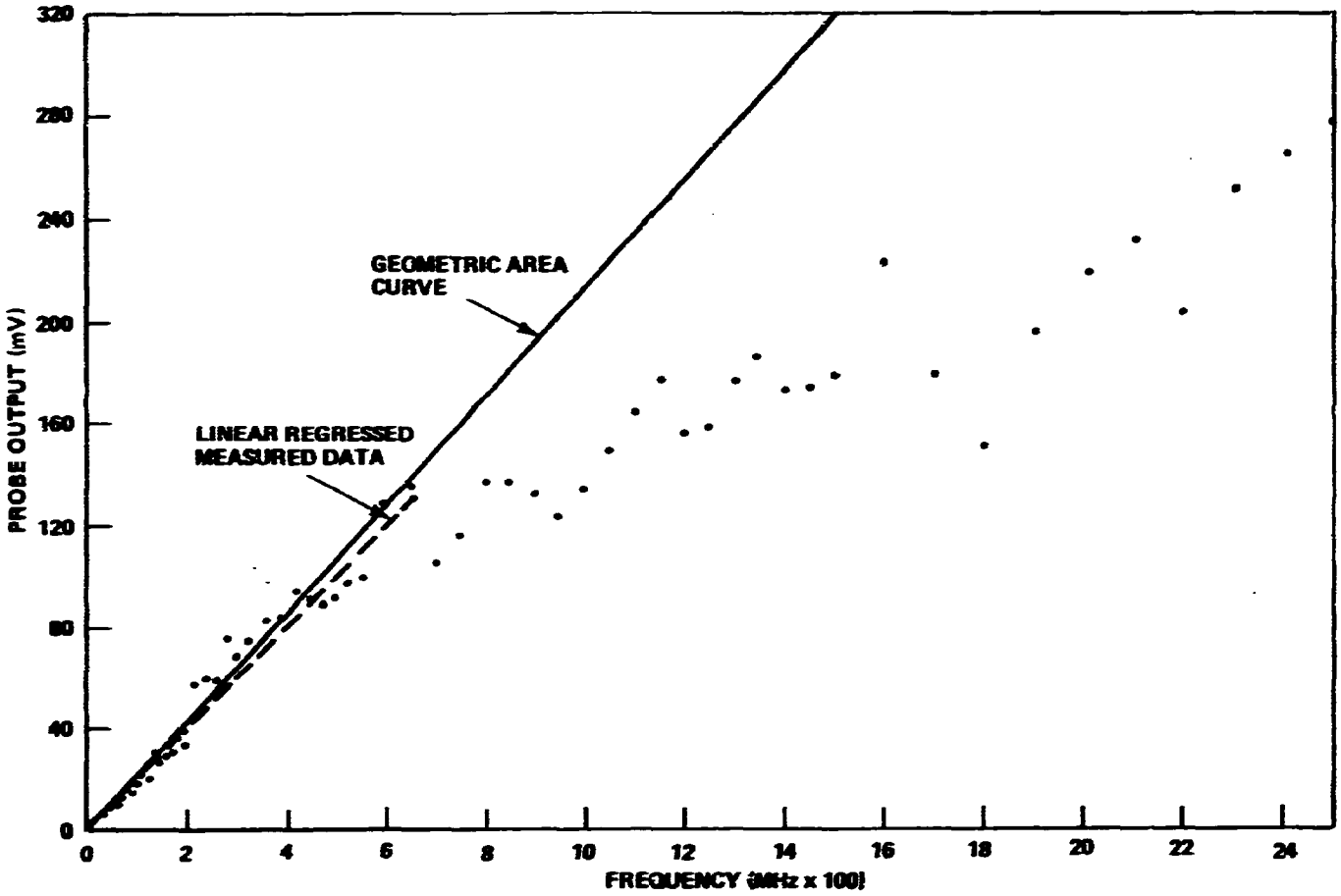

Figure 33. Calibration curve for 1-in. single-gap B dot sensor, E_0 = 20 V/m.

TABLE 2. RESULTS OF LINEAR REGRESSION OF SENSOR CALIBRATION DATA

Probe Tested	Upper Frequency of Linear Regression (MHz)	Linear Regression Parameters							Probe Area (m^2)		Efficiency (%)
		a_0 (mV)	a_1 (mV/MHz)	r^2	$\hat{y}$	$S_{y \cdot x}$	S_0	$S_1 \times 10^{-3}$	$A_{eq} \times 10^{-4}$	$A_G \times 10^{-4}$	
Single gap											
1-in. diameter	650	0.4556	0.2022	0.9650	0.6519	6.873	2.070	6.707	4.82	5.07	95.2
1.5-in. diameter	650	14.11	0.3909	0.9690	1.449	12.66	3.812	12.35	9.33	11.4	81.9
Double gap											
0.875-in. diameter	2500	1.39	0.07739	0.9737	1.4680	9.0940	1.7436	1.6554	1.85	1.76	—
1.75-in. diameter	1150	14.07	0.2899	0.9455	14.35	23.37	5.6069	10.736	6.92	7.39	94

The voltage calculation for the 1.5-in. single-gap B dot sensor regression (Table 2) to 650 MHz is as follows:

$$V_p = 14.11 \text{ mV} + 0.39089 \text{ mV/MHz} \times 650 \text{ MHz} = 268.2 \text{ mV at } 650 \text{ MHz}.$$

The dotted line on Figure 24 displays these data.

The voltage calculation for the 7/8-in. double-gap B dot sensor regression (Table 2) to 2.5 GHz is as follows:

$$V_p = 1.39 \text{ mV} + 0.077392 \text{ mV/MHz} \times 2500 \text{ MHz} = 193.5 \text{ mV at } 2500 \text{ MHz}.$$

This linear regressed line is the dotted line on Figure 23.

The voltage calculation for the 1.75-in. double-gap B dot sensor linear regression (Table 2) is as follows:

$$V_p = 14.07 \text{ mV} + 0.28985 \text{ mV/MHz} = 347.4 \text{ mV at } 1150 \text{ MHz}.$$

This is the dotted line shown on Figure 22. Although the linear regression was terminated at 1150 MHz, the data show the probe to be excellent all the way to 2500 MHz.

B. 50-MHz to 1-GHz Calibrating of B Dot Sensors Using NBS Standard Dipoles

The previous calibrations of the B dot sensors below 1 GHz was accomplished using the adjustable dipoles with a guaranteed accuracy of ±3 dB. To obtain a much more accurate calibration, the 1.75- and 3.5-in. B dots were calibrated using the NBS standard dipoles to set up known standard fields. These fields were normalized to 1 V/m. The B dot measured fields using only cable correction factors are plotted in Figure 34. This figure indicates as large as a 30% error in the B dot field measurement. The data were normalized to 1 V/m by using the normalization factor shown in Table 3. Simplifying the basic B dot equation one can write

$$E_o = C_p V_p \quad , \tag{23}$$

where

E_o = electric field

C_p = constant associated with a particular frequency

V_p = probe output in millivolts (normalized to $E_o = 1$) ;

then

$$C_p = \frac{1}{V_p} \quad . \tag{24}$$

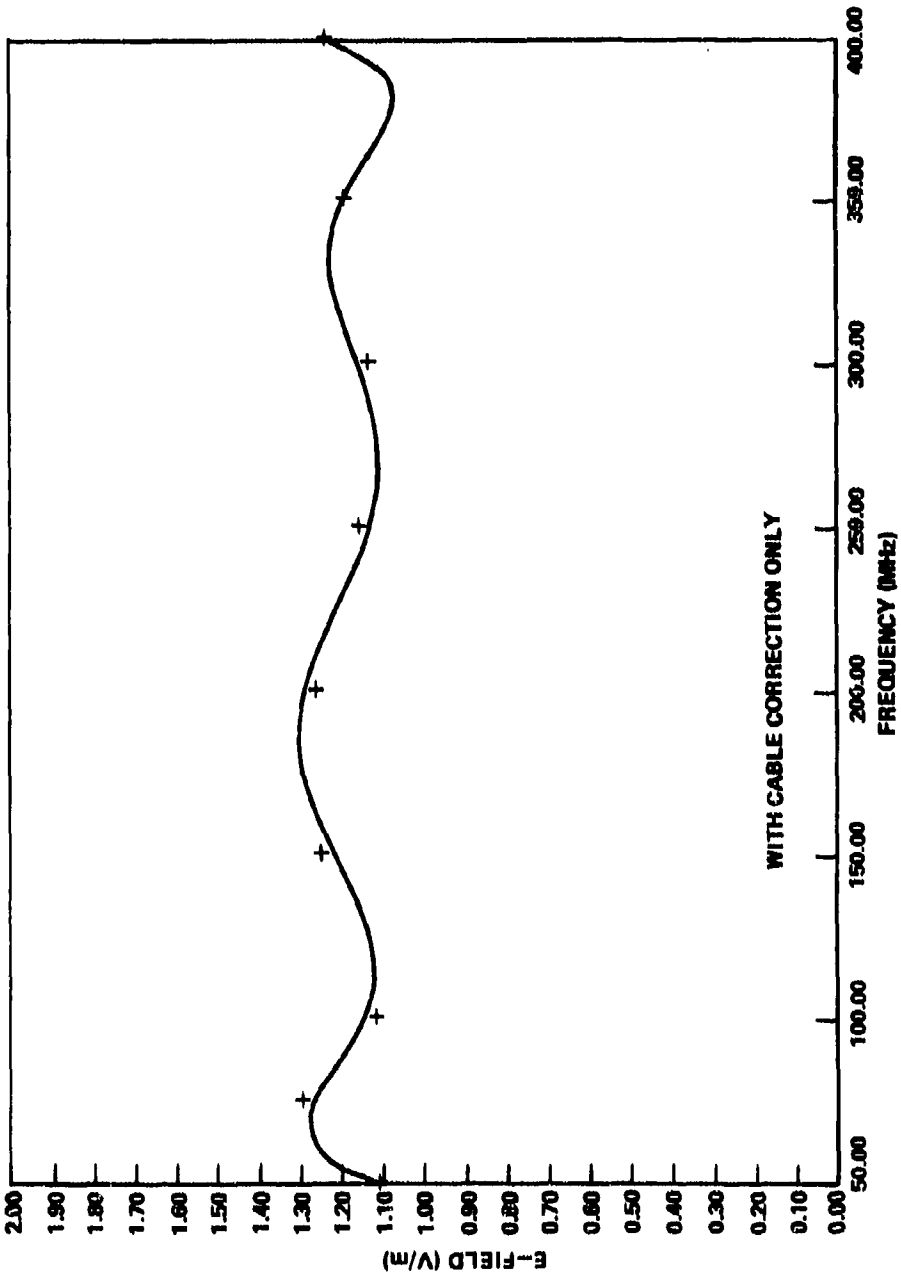

Figure 34. B dot E-field plot using cable correction.

TABLE 3. 3.5-IN. DIAMETER B DOT NORMALIZATION FACTORS

Frequency (MHz)	NBS Dipole (V/m)	1 V/m Normalization Factor	Normalized B Dot Output (mV)	C_p
50	0.063	15.87	3.17	0.315
75	0.082	12.20	5.61	0.178
100	0.124	8.06	6.05	0.165
150	0.138	7.25	10.30	0.097
200	0.205	4.88	13.18	0.072
250	0.267	3.75	15.00	0.067
300	0.333	3.00	17.40	0.057
350	0.223	4.48	21.06	0.047
400	0.479	2.07	25.25	0.040

C. Calibration Procedure and Data

The procedure used to calibrate the B dot probe is the direct substitution method; i.e., the standard field was established using the NBS standard dipoles. The probe is then substituted in the exact position of the standard dipole. The output of the probe is then read using a power meter or a calibrated RF voltmeter. The normalized probe output C_p is plotted versus frequency in Figure 35. Table 4 and Figure 36 give C_p for the 1.75-in. probe.

D. Development of Calibration Factors and Calibration Polynomial

To improve the accuracy of the B dot probe to better than the 30% error shown in Figure 34, the necessary calibration polynomials were developed. First, the probe was placed in a standard field as determined by the NBS standard dipoles. The data were then normalized to 1 V/m by using the normalization factor shown in Tables 3 and 4. Recall Equation (23),

$$E_o = C_p V_p \quad ,$$

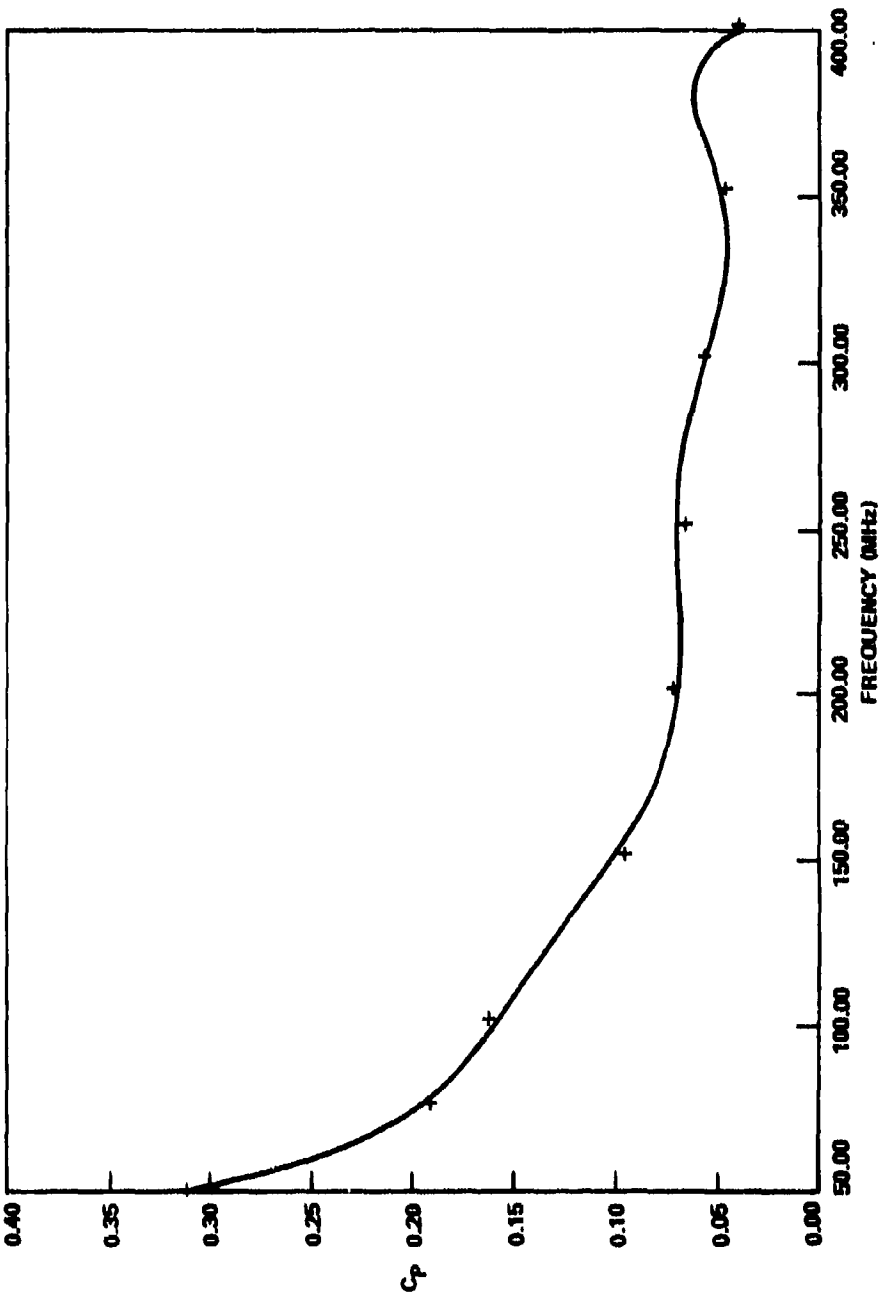

Figure 35. C_p versus frequency for 3.5-in. B dot probe.

TABLE 4. 1.75-IN. DIAMETER B DOT NORMALIZATION FACTORS

Frequency (MHz)	NBS Dipole (V/m)	1 V/m Normalization Factor	Normalized B Dot Output (mV)	C_p
500	3.7	0.270	6.33	0.158
600	4.45	0.225	8.71	0.115
700	5.2	0.192	9.60	0.104
800	5.9	0.169	10.07	0.099
900	4.7	0.213	13.13	0.076
1000	3.7	0.270	11.61	0.086

where C_p is a constant associated with a particular frequency. Since E_o has been normalized to $E_o = 1$, then Equation (24) becomes

$$C_p = \frac{1}{V_p} \quad ,$$

which is shown in Tables 3 and 4.

Using this factor, C_p, one can develop the frequency dependent polynomial (C_p) which can be used by the computer to make the output of the B dot agree with the NBS standards.

Using the Hewlett-Packard Model 9830 computer polynomial program and the data from Tables 3 and 4, the values for C_p are plotted versus frequency. These data are then used to develop the polynomial (C_p). The coefficients for (C_p) of a 3.5-in. probe from 50 to 400 MHz are as follows:

B (0) = 1.926957 +00

B (1) = -7.392284 E -02

B (2) = 1.316170 E -03

B (3) = 1.260325 E -05

B (4) = 6.878694 E -08

B (5) = -2.140627 E -10

B (6) = 3.534933 E -13

B (7) = 2.403270 E -16.

The coefficients for a 1.75-in. probe from 500 MHz to 1 GHz are as follows:

B (0) = 6.952785 E +00

B (1) = 5.844569 E -02

B (2) = 1.840281 E -04

B (3) = 2.792819 E -07

B (4) = 2.058278 E -10

B (5) = 5.916707 E -14.

The plot of the data and the polynomial curves are shown in Figures 30 and 31. The general equation then becomes

$$E_o = (C_p)\ V_p \quad , \tag{25}$$

where (C_p) is the frequency dependent polynomial and V_p is the probe output in millivolts. Figure 1 gives the error of the 3.5-in. probe with no calibration corrections. This graph is typical but is not the same for all 3.5-in. probes. Construction tolerances cause each probe to have different output characteristics.

E. Recommendation

To assure accuracies of better than ±1 dB, it is recommended that the probe be calibrated against the NBS standard antennas. Uncalibrated probes have errors greater than 1 dB. It is further recommended that the 3.5-in. probe be used below 400 MHz and the 1.75-in. probe be used from 400 MHz to 1 GHz. It is possible to calibrate the 3.5-in. probe to higher frequencies; however, the patterns and outputs are not as predictable and the calibrations are more difficult.

Use of B dot as a standard field measuring probe has given rise to a need for a ruggedized probe. The development of a more durable probe would save considerable time on repair and checkout of damaged probes.

It should be reiterated that these measurement techniques preferred in this study are applicable to uniform planar E fields (i.e., farfield environment). However, the usefulness of these probes is not limited to the previously mentioned applications, provided these techniques are modified to account for the nonplanarity of the field. These modifications would require an accurate characterization of B and E fields. An area of E field research which can be explored utilizing the B dot probe is near-field characterization of antennas. The B dot antenna along with calibrated dipoles could be used to measure the orthogonal components of the E and B fields. These measurements can then be used to determine the power densities in close proximity to high power antennas.

REFERENCES

1. Mory, Res, et al, Development and Production of Multi-Gap Loop (MGL) Series EMP B Dot Sensors, EMP 1-2, Air Force Weapons Laboratory, AFWL-SRE, Kirtland AFB, New Mexico, February 1971, Technical Report No. AFWL-TR-70-153.

2. Baum, C. E., "Maximizing Frequency Response of a B Dot Loop," Electromagnetic Pulse Sensor and Simulation Notes, Vol. I, Note 8, Air Force Weapons Laboratory, June 1970, Contract No. F29601-70-C-0010.

3. Whiteside, H. and King, R. W. P., "The Loop Antenna as a Probe," IEEE Transaction on Antenna and Propagation, May 1964, pp. 291-297.

4. Baum, C. E., "A Conical - Transmission - Line Gap for a Cylindrical Loop," Electromagnetic Pulse Sensor and Simulation Notes, Vol. 2, Air Force Weapons Laboratory, AFWL-WLRE, Kirtland AFB, New Mexico, June 1970, AFWL EMP 1-2.

5. Baum, C. E., "The Multi-Gap Cylindrical Loop in Non-Conducting Media," EMP Sensor and Simulation Note 41, Air Force Weapons Laboratory, June 1970, AFWL EMP 1-2, Vol. 2, Contract No. F29601-70-C-0010.

6. Saad, T. S., Microwave Engineering Handbook, Vol. I, Aertech House, Inc., 1971.

7. Kerr, John L., Broadband Horns, US Army Electronics Command, August 1970, ECOM-3319.

8. Kerr, John L., "Short Axial Length Broadband Horns," 22 Annual Symposium on US Air Force Antenna Research and Development, October 1972.

9. Draper and Smith, Applied Regression Analysis, John Wiley & Sons, New York, 1966.

10. Ostle, B., Statistics in Research, Iowa State University Press, Iowa City, Iowa, 1963.

11. Baum, C. E., "A Technique for the Distribution of Signal Inputs to Loops," Electromagnetic Pulse Sensor and Simulation Notes, Vol. I, Note 23, Air Force Weapons Laboratory, Kirtland Air Force Base, New Mexico, Contract No. F29601-70-C-0010, June 1970, AFWL-EMP 1-1.

12. Taggart, Harold E. and Workman, John L., Calibration Principles and Procedures for Field Strength Meters (30 MHz to 1 GHz), March 1969, NBS Technical Note 370.

DISTRIBUTION

	No. of copies
Defense Documentation Center Cameron Station Alexandria, Virginia 22314	12
Commander US Army Materiel Development and Readiness Command	
ATTN: DRCRD	1
DRCDL	1
5001 Eisenhower Avenue Alexandria, Virginia 22333	
DRSMI-LP, Mr. Voigt	1
DRDMI-ETR, Mr. Edlin	20
-T, Dr. Kobler	
-TBD	3
-TI (Record Set)	1
(Reference Copy)	1